Results in Chemistry 16 (2025) 102486

Contents lists available at ScienceDirect

Results in Chemistry

journal homepage: www.sciencedirect.com/journal/results-in-chemistry

Synthesis of diatomite/Fe_3O_4/Teff straw activated carbon composite adsorbent for Cr(VI) removal from wastewater

Sintayehu Shewatatek [a], Girma Gonfa [a,b,c,*], Sintayehu Mekuria [a,b], Belete Tessema [a], Gulmira Kezembayeva [d], Kalyan Sundar Ghosh [e], Muhammad Mushtaq [f,**], Mohammad Hadi Diyanatizadeh [g], Kaan Isinkaralar [h], Ahmad Hosseini-Bandegharaei [i,j,k,***]

[a] Department of Chemical Engineering, Addis Ababa Science and Technology University, 16417 Addis Ababa, Ethiopia
[b] Biotechnology and Bioprocess Center of Excellence, Addis Ababa Science and Technology University, 16417 Addis Ababa, Ethiopia
[c] Nanotechnology Center of Excellence, Addis Ababa Science and Technology University, 16417 Addis Ababa, Ethiopia
[d] Mining and Metallurgical Institute named after O.A. Baikonurov, Department Chemical Processes and Industrial Ecology, Satbayev University, Almaty, Kazakhstan
[e] Department of Chemistry, National Institute of Technology Hamirpur, Hamirpur, India
[f] Department of Chemistry, Government College University Lahore, Pakistan
[g] Research & Development Division, Zarmehr Tehran Oxin Co., Shahrak Gharb (Ghods), Tehran 1468943815, Iran
[h] Department of Environmental Engineering, Faculty of Engineering and Architecture, Kastamonu University, Kastamonu 37150, Türkiye
[i] Faculty of Chemistry, Semnan University, Semnan, Iran
[j] Research and Innovation Cell, Rayat Bahra University, Mohali, Punjab, India
[k] Department of Sustainable Engineering, Saveetha School of Engineering, SIMATS, Chennai 602105, Tamil Nadu, India

ARTICLE INFO

Keywords:
Magnetic composite adsorbent
Chromium (VI) adsorption
Diatomite
Teff straw waste
Adsorption properties
Sustainability

ABSTRACT

Heavy metal pollution, particularly chromium (Cr), poses a significant environmental challenge. This study addresses this issue by developing a novel composite adsorbent consisting of diatomite (DE), Fe_3O_4, and an activated carbon from teff straw (TSAC). The nanocomposite was characterized, exploiting FT-IR, BET, SEM, and XRD analyses, revealing a substantial BET surface area of 347.45 m^2/g. Response surface methodology (RSM) with central composite design (CCD) was exploited to optimize adsorption parameters, including pH, adsorbent dose, initial Cr(VI) concentration, and adsorption time. Optimal conditions yielded a removal efficiency of 93.28 % at pH 4, an adsorbent dose of 0.024 g/100 mL, an initial Cr(VI) level of 15 mg/L, and an adsorption time of 60 min. The results showed that the Freundlich and Langmuir isotherm models, along with Toth model, best matched the data. This implies that both monolayer and heterogeneous surface adsorptions are the main mechanism, with a maximal sorption capacity of 131 mg/g and followed the pseudo-second-order kinetic model. Thermodynamic analyses uncovered the spontaneous and endothermic nature of the Cr (VI) adsorption by DE/Fe_3O_4/TSAC. The composite's recyclability was demonstrated over five cycles, maintaining significant removal efficiency. Such findings highlight the potentials of the DE/Fe_3O_4/TSAC composite for effective Cr (VI) removal from water, offering a promising solution to mitigate chromium pollution.

1. Introduction

A common inorganic contaminant, chromium naturally exists in a variety of oxide forms, such as crocoite and chromite. The environmental impact of chromium makes these compounds important. A significant source of chromium is chromite, which is mainly made up of iron and chromium oxides, whereas lead chromate is found in crocoite. Chromium's extensive distribution and environmental concerns are a result of its several oxidation states [1]. Chromium is also generated by human endeavors, notably nuclear power plants and various metallurgical processes [2], electroplating processes [3], tanning processes [4], and chromium metal production, contributing to its environmental presence. Chromium mostly is present as chromium (III) and chromium (VI) oxidation states [5]. Cr (VI) is remarkably more toxic than Cr (III)

* Corresponding author at: Department of Chemical Engineering, Addis Ababa Science and Technology University, 16417 Addis Ababa, Ethiopia.
** Corresponding author at: Department of Chemistry, Government College University Lahore-Pakistan
*** Corresponding author at: Faculty of Chemistry, Semnan University, Semnan, Iran.
E-mail addresses: kiyyaagonfaa@gmail.com (G. Gonfa), muhammad.mushtaq@gcu.edu.pk (M. Mushtaq), ahoseinib@yahoo.com (A. Hosseini-Bandegharaei).

https://doi.org/10.1016/j.rechem.2025.102486
Received 19 March 2025; Accepted 1 July 2025
Available online 5 July 2025

owing to its higher solubility and mobility in water [6]. In water, chromium exists as oxyanions like hydrogen chromate ($HCrO_4^-$) [6], dichromate ($Cr_2O_7^{2-}$) [3], and chromate (CrO_4^{2-}), depending upon pH levels; it is present as $HCrO_4^-$ and $Cr_2O_7^{2-}$ in acidic conditions, and as CrO_4^{2-} in basic conditions. This makes removing Cr(VI) from water bodies difficult [7].

Chromium salts are the primary chemical source used in tanning industries [5]. Globally, a large amount of chromium is released into water bodies from the tanning process, significantly increasing the levels of Cr(VI) in aquatic environments [2]. The global leather industry discharges substantial amounts of wastewater (over 300 million tons) [2], posing significant threats to human health and aquatic ecosystems [8]. Rapid urbanization and industrialization exacerbate this issue by releasing large quantities of untreated pollutants, including hexavalent chromium, into water bodies [8]. For example, recent research by Fito and colleagues [8] shows that Batu Tannery PLC in Ethiopia releases an alarming amount of hexavalent chromium (Cr(VI)) into local water resources, with concentrations reaching 85.13 ± 1.22 mg/L. This level far exceeds the World Health Organization's (WHO) guidelines, which set the maximum acceptable limit at 0.05 mg/L for drinking waters and 0.2 mg/L for wastewaters [9]. Above these threshold limits, Cr(VI) can bring about severe health problems such as kidney dysfunction [6], nerve tissue damage processes [4], liver damage [10], and carcinogenic [8]. Hence, it is critical to retrieve excess Cr (VI) from water bodies.

To date, many techniques have been used to remove Cr(VI), including precipitation [11], coagulation [12], membrane separation [13], oxidation-reduction [14], and adsorption [15]. Among these methods, adsorption is preferred by the virtues of its simple design, ease of operation, and low-cost [16]. Additionally, adsorption utilizes various low-cost and readily available adsorbents such as clays, agricultural wastes, biochar, activated carbon and polymers [16,17].

In this research, the exploitation of diatomite (DE), teff straw-derived activated carbon and Fe_3O_4-based composite sorbent was brought under scrutinization for removal of Cr(VI) from waters. Raw DE was cleaned and treated with H_2SO_4 to remove impurities and improve its surface activities. Naturally occurring DE contains impurities of the mineral and organic compounds that cause insufficient wettability, fewer available reaction sites, and poor regenerations [18]. Activated carbon was prepared from Teff (*Eragrostis tef*) straw by calcinating at an elevated temperature after treating it with H_3PO_4. The Teff straw is a lignocellulosic material and is found as a residue after seeds are removed [19]. Teff make up over 25 % of all crop products produced in Ethiopia [19]. Teff straw-derived activated carbon (TSAC) has special qualities such as a wide surface area, [20], high carbon content [21], surface-enriched functional group [22], and stable structure [23] and a great ability to remove both organic and inorganic contaminants and particularly has high adsorption capacity for Cr (VI) removal [19]. Despite its unique properties it still has regeneration challenges and creates secondary pollutants [21]. Additionally, its adsorption capacity for anionic contaminants is limited owing to electrostatic repulsions, hindering effective removal [24]. These limitations significantly limit the exploitation of TSAC for removing Cr (VI) from aqueous solutions. Hence, magnetite (Fe_3O_4) was incorporated into the composite to improve its affinity for Cr(VI) and improve chromium adsorption capacity and further reducing Cr(VI) to a lesser poisonous Cr(III) form [8]. In this context, some studies have already reported on the application of binary composites of DE/Fe_3O_4, biochar/Fe_3O_4, and DE/Cellulose to improve Cr(VI) adsorptive uptake from waters [8,25]. For instance, Lemessa, Chebude [25] have enhanced the sorption capacity of natural DE for Cr(VI) by loading it with magnetic nanoparticles. Moreover, Fito, Abewaa [8] have observed the combination of BC (biochar) with Fe_3O_4 to improve recyclability of a prepared composite of BC/Fe_3O_4 for Cr(VI) adsorption from contaminated waters. However, to our knowledge, no studies have been conducted for retrieving Cr(VI) from waters and wastewaters using the ternary composites of DE/Fe_3O_4/TSAC. The combination of DE/Fe_3O_4/TSAC materials possibly enhances several active sites such as hydrophobicity, hydrophilicity, and surface charge. Diatomite's primary role is to provide structural support and enhance the dispersibility of the other components, preventing aggregation and improving the overall stability and porosity of the composite [26]. Fe_3O_4 magnetic nanoparticles (MNPs) as efficient adsorbents have been utilized for heavy metal adsorption on due to low toxicity, large specific surface area and superparamagnetic property contributes to the reduction of Cr (VI) to the less toxic Cr (III) form through redox reactions [27].Teff straw activated carbon provides a high surface area and abundant adsorption sites for Cr (VI) removal [28]. This study involved synthesizing a composite adsorbent, DE/Fe_3O_4/TSAC, with varying DE/TSAC ratios. The adsorbent was tested for its efficacy in removing Cr (VI) from aqueous solutions. The adsorption process was analyzed, exploiting isotherm and kinetic models, while factors like initial Cr (VI) concentration, solution pH, adsorbent dosage, and contact duration were evaluated by experimental design. Thermodynamic computations were adopted to assess the feasibility of the adsorption process. The findings provided valuable insights into the optimal conditions for efficient Cr (VI) removal, highlighting the potential of this composite adsorbent in environmental remediation applications.

2. Materials and methods

2.1. Materials and reagents

Raw diatomite samples [7] were collected from Adami-Tulu, Ethiopia, situated 168 km southeast of Addis Ababa. Teff straw [5] was obtained from a farm in Addis Ababa, Ethiopia. Ferric chloride hexahydrate ($FeCl_3.6H_2O$), sulfuric acid (98 %), hydrochloric acid (37 %), phosphoric acid (85 %), sodium hydroxide (98 %), sodium chloride, potassium dichromate (99 %), acetone (99.9 %), nitric acid, sodium acetate (99.5 %), ethylene glycol, and 1, 5-diphenylcarbazide (85 %) were obtained from Sigma Aldrich. All chemicals and reagents employed in this study were of the highest analytical quality and were utilized directly, without undergoing additional purification processes.

2.2. Apparatus and equipment

Surfaces' morphologies were scrutinized by exploiting a SEM microscope (scanning electron microscope; Inspect F50, USA) at desirable magnifications, with a 15-kV voltage. The specific surface area of the magnetic composite adsorbent was calculated by BET (Brunauer-Emmett-Teller; SA 9600 instrument) method, while FTIR (Fourier-Transform Infrared) spectroscopy (using a Nicolet iS50 instrument) was employed to identify the functional moieties within the wavenumbers span of 4000 and 400 cm^{-1}. The magnetic composite adsorbent's crystallinity was examined using a Cu Kα radiation source in an X-ray diffractometer (XRD-7000, Shimadzu Co., Japan) that scanned a range of angles from 10° to 80° with a temporal step. The concentrations of Cr (VI) ions in the water were measured by exploiting a UV–Vis spectrophotometer (UV-1800, Shimadzu).

2.3. Adsorbent preparations

2.3.1. Diatomite preparation

The raw diatomite (RDE) was first cleaned with deionized water and dried in an oven for 24 h at 105 °C. It was then pulverized in a disc mill and sieved through a 69 μm sieve. The sample was then treated with 4 M hot H_2SO_4 for 10 h at DE to acid ratio of 50 g/L at temperature of 90 °C. A magnetic stirrer was exploited to agitate the mixture at 1000 rpm. Then, the acid treated DE was separated using vacuum filtration, and the sample was rinsed with distilled water until the pH reached a neutral level. The sample dried for 12 h at 105 °C in an oven and kept in a tightly sealed container until further usage.

2.3.2. Activated carbon production

The teff straw was sorted to remove contaminants and soaked in tap water overnight. Then, it was rinsed three times with deionized water and dried under the sunlight. Afterward, it was milled and was treated with 3 M H_3PO_4 for 24 h under continuous mixing. The impregnation ratio (weight of Teff straw to weight of phosphoric acid) was of 1:5674 (g/g). Following impregnation, the samples were carefully dried outdoors, exposed to natural sunlight, and then thermally treated 453.92 °C for two h at a heating rate of 10 °C/min underneath nitrogen flow rate of 180 cm^3/min in a muffle furnace. After thermal treatment, the samples cooled down cleated with distilled water until the pH of the cleaning water stabilizes at a neutral pH of 7.0. The samples dried at 100 °C (for 12 h) in an oven and kept sealed container until further use.

2.3.3. DE/Fe3O4/ TSAC composite adsorbent preparation

One gram of teff straw activated carbon was added to a 25-mL portion of nitric acid solution (6 M). The mixture was then heated under reflux conditions at the boiling point for a duration of 100 min. HNO_3 was used to oxidize the activated carbon [29]. The mixture was cooled and subsequently AC was rinsed with deionized water until it reached a neutral pH. Following, the oxidized activated carbon was oven-dried in vacuum for 24 h at 65 °C. Next to synthesize a magnetic composite adsorbent from treated diatomite, oxidized activated carbon, and magnetite. $FeCl_3.6H_2O$ (3 g), NaAC (6.0 g), at various mass ratios of treated diatomite/ oxidized activated carbon (0.4:1.2, 1.2:0.4, 0.8:0.8) dispersed in of ethylene glycol (100 mL) with gentle agitation for 1 h. The prepared solution was poured into a Teflon-lined stainless-steel autoclave and subjected to thermal treatment at 200 °C for 8 h as shown in Fig. 1. After allowing the autoclave to cool naturally to ambient temperature, the resulting product was retrieved by exploitation of a magnet and thoroughly washed multiple times with ethanol and water to ensure purity. Finally, the material was vacuum-dried at 60 °C for 24 h to acquire the final sorbent [29].

2.4. Adsorption experiment

2.4.1. Point of zero-point of charge (pHpzc)

The acid-base titration procedure was exploited to examine the synthesized materials' point of zero charge [30]. In this procedure, six Erlenmeyer flasks holding 50 mL of 0.1 M NaCl were filled with 1 g of the DE/FeO_4/TSAC composite adsorbent. Using 0.1 M NaOH or 0.1 M HCl, the pH of the solutions was adjusted between 2 and 12, and an orbital shaker (SSL1, UK) was used to shake the solution. After 48 h, the solution's pH was finally measured, and pH pzc was computed by overlapping the pH initial and pH final curves [30].

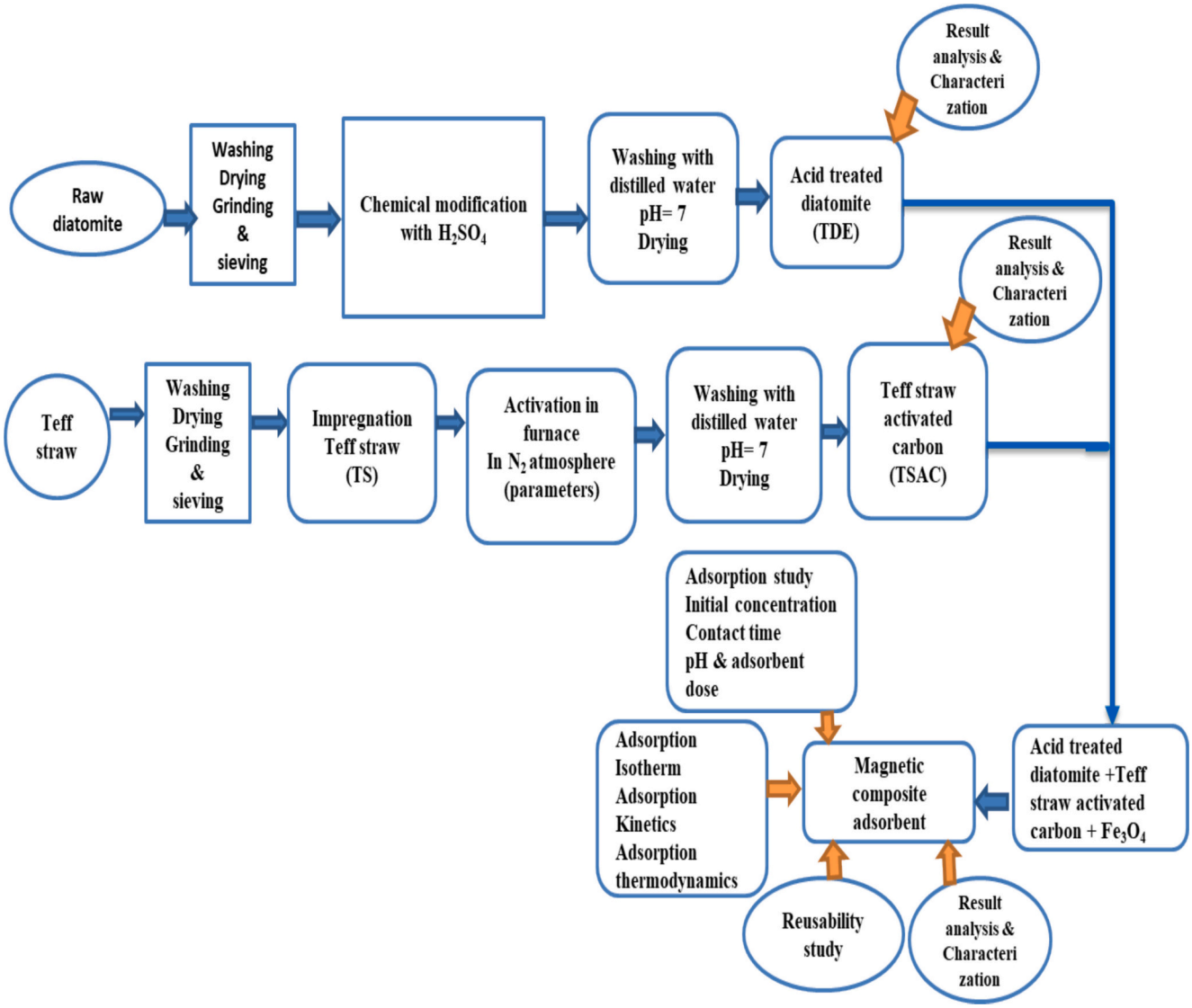

Fig. 1. Synthesis of TDE / Fe_3O_4/ TSAC adsorbent by solvothermal method.

2.4.2. Fabrication of standard solutions

Prior to preparing the standard solutions, a stock solution (1000 ppm) was built by desolation of 2.8280 g of $K_2Cr_2O_7$ in 1 L of distilled water. Nine standard solutions (0.2, 0.4, 0.6, 0.8, 1, 3, 5, 7, and 9 mg/L) were built by adding the $K_2Cr_2O_7$ solution to 100 mL flasks. Next, in a meticulous procedure, each standard solution was carefully treated with 2 mL of freshly prepared 1,5-diphenylcarbazide (1,5-DPC). This initial step was followed by the addition of 5 mL of 0.2 N sulfuric acid (H_2SO_4), which served to acidify the mixture. Almost instantaneously, a striking pink-red hue blossomed within the solution, vouchsafing the formation of the chromium-DPC complex. With precision, each flask was then filled to its calibration mark using distilled water, effectively creating the final Cr(VI) solution. The careful preparation culminated in the spectroscopic analysis, where each sample' absorbance was read by a UV–visible spectrometer. The wavelength of maximum absorption (λ_{max}) was determined to be 540 nm, corresponding to the characteristic absorption peak of the chromium-DPC complex.

2.4.3. Adsorption parameter study

The effects of each of the following variables were examined: pH, adsorbent dose, beginning Cr (VI) level, and contact time. Different amounts (0.01, 0.015, 0.02, 0.025, and 0.03 g) of DE/Fe_3O_4/TSAC composite adsorbent were introduced to a 100-mL volumetric flask containing 20 mg/L of adsorbate (Cr (VI)) in order to appraise the impact of the nanocomposite dosage. The obtained suspensions were agitated for 60 min at 150 rpm, exploiting an orbital shaker [31]. The DE/Fe_3O_4/TSAC was separated from the solution by filtering it after shaking. 0.025 g of DE/Fe3O4/TSAC was added to a solution containing 20 mg/L of adsorbate (Cr(VI)) while adjusting the pH levels (2.0, 4.0, 6.0, 8.0, and 10.0), exploiting 0.1 M HCl and 0.1 M NaOH solutions in order to assess the impact of pH on Cr(VI) removal. After 60 min of shaking at 150 rpm, the mixture was filtered. Batch adsorption experiments were conducted to investigate the removal of Cr(VI) under varying initial concentrations and contact times. The initial Cr(VI) concentrations were set at 10, 15, 20, 25, and 30 mg/L. The suspensions were shaken for 60 min at a speed of 150 rpm, followed by filtration. To evaluate effects of contact duration on sorption, experiments were performed at intervals of 5, 15, 30, 45, 60, and 75 min under identical shaking conditions (150 rpm). After filtration, the filtrates were treated with 2 mL of 1,5-diphenylcarbazide (1,5-DPC) and 5 mL of 0.2 N H_2SO_4 to develop a pink-coloured solution. The levels of Cr(*VI*) in the filtrates were analyzed by exploiting a UV–Visible spectrophotometer (UV-1800, Shimadzu) at the suitable wavelength (540 nm). The removal efficiency (R%) and adsorption capacity were calculated by exploitation of appropriate expression (Eqs. (1) and (2) to quantify the adsorption performance [32–34].

$$Removal\ Efficency\ (\%) = \frac{Co - Ce}{Co} * 100\% \quad (1)$$

The percentage of chromium or methyl orange removal will be calculated using Equation

$$Adsorption\ capacity = \frac{Co - Ce}{m} V \quad (2)$$

where V is the volume of the Cr(VI) solution, Ce is the equilibrium concentration of chromium, Co is the starting concentration, and m is the mass of the adsorbent.

2.4.4. Experiential design

In this work, the adsorption process parameters for the removal of Cr (VI) from aqueous solution were improved by the application of Response Surface Methodology in a Central Composite Design (CCD). Applying the RSM technique to quantitative experimental data in this case resulted in a model equation and the optimal condition for the adsorption process. RSM that made it particularly suitable for our research objectives, such as its efficiency in simultaneously evaluating multiple factors and their interactions, its ability to model complex non-linear relationships, and its capacity to generate a comprehensive response surface for understanding the process behaviour. In order to maximize the process four crucial variables were chosen: adsorbent dosage (A), solution pH (B), contact time (C), and initial Cr (VI) level (D), were thoroughly examined [33,34]. The response was defined as the percentage of Cr (VI) ion removed. The levels and ranges of the selected independent variables are shown in Table 1.

The CCD-based RSM's necessary number of experimental points can be computed by

$$2^n + 2n + c;$$

where; n is the independent factors (parameters) and *c* is the number of center points.

$$y = \beta_0 + \sum \beta_i x_i + \sum \beta_{ii} x_i^2 + \sum \beta_{ij} x_i X_j \quad (3)$$

where xi is the independent factor (adsorbent dosage (A), solution pH (B), contact time (C), and initial Cr (VI) level (D)), y is the Cr(VI) removal effectiveness (%), and βi is the coefficient.

2.4.4.1. Statistical analysis. Employment of Response Surface Methodology in optimizing the conditions for Cr(VI) removal is a sophisticated technique that combines experimental design with mathematical and statistical modeling. By creating a quadratic model, RSM is able to slice through the complexity of multi-variable interactions to predict the optimum conditions for maximum removal efficiency. The use of Central Composite Design (CCD) in creating experimental data points ensures a thorough exploration of the variables at hand. The optimization process through Design-Expert software illustrates the practical application of RSM, where it provides a user-friendly interface to optimize the model and its validation. ANOVA is important in this context as it statistically validates the model's accuracy, which renders the predictions reliable. Lastly, the 3D surface plots offer the graphical representation of the interaction effects, providing intuitive insight into how different variables interact to affect the response. This exhaustive methodology serves to demonstrate the power of statistical modeling for environmental engineering, particularly in the important process of pollutant removal.

2.4.4.2. Model validation. The batch adsorptive experiment results were also compared with the predicted values of the RSM model, which provides a relationship between certain parameters and the Cr(VI) removal efficiency, to check the validity of the model. One of the valid statistical methods frequently used for optimization of complex processes is the Response Surface Methodology. RSM can prove useful in identifying the impact of certain parameters such as initial pH, amount of the adsorbent, contact time, and initial concentration of Cr(VI) on the process efficiency to remove Cr(VI). The study shows that under RSM, optimum conditions can be achieved which are effective for maximum removal of Cr(VI).

2.5. Adsorption kinetics, isotherms and thermodynamics

The interaction between adsorbates and the surface of adsorbents, along with the mechanisms governing their adsorption, can be effec-

Table 1
Levels and ranges of the independent variables utilized in the design of the experiment.

Range and level			
Parameters	−1	0	1
Adsorbent dosage	0.02	0.03	0.04
Solution pH	4	6	8
Contact time	30	45	60
Initial Cr (VI)	15	10	25

tively analyzed using various kinetic models. The tested models comprise of the pseudo-first-order, pseudo-second-order, and intra-particle diffusion models. Each model provides insight into different aspects of the adsorption process [11]:

$$\text{Pseudo} - \text{first order } q_t = q_e.\left[1 - exp^{(-K_1.t)}\right] \quad (3)$$

$$\text{Pseudo–second order } q_t = \frac{{q_{e2}}^2.K_2.t}{[K_2.(q_{e2}).t + 1]} \quad (4)$$

$$\text{Intraparticle diffusion} q_t = k_p t^{0.5} + c \quad (5)$$

where q_t is the Cr(VI) amount sorbed on the sorbent surface in (mg/g), q_e is its amount sorbed on DE/Fe_3O_4/TSAC surface at equilibrium (mg/g), at time t [6], k_1 and k_2 are the first and second pseudo-order rate constants (min^{-1}), respectively, k_p is the intraparticle diffusion constant (mg (g min0.5)$^{-1}$), and c (mg/g) is the boundary layer's thickness that indicates the resistance to the mass transferring.

Langmuir, Freundlich isotherm, and Temkin isotherm models (two-parameter models), along with three three-parameter models, that is, Sips and Redlich-Peterson models were studied to investigate adsorption mechanisms on the DE/Fe_3O_4/TSAC surface.

$$q_e = \frac{Q_{max} + K_L C_e}{1 + K_L C_e} \quad (6)$$

The Langmuir model (non-linear form)

$$\text{The Freundlich isotherm model } q_e = K_f C_e^{\frac{1}{n}} \quad (7)$$

$$\text{The Temkin isotherm model} q_e = \frac{RT}{b}\left(\ln K_T C_e\right) \quad (8)$$

$$\text{The Sips isotherm model} q_e = \frac{q_{max}\left(K_S.C_e\right)^{1/n}}{1 + \left(K_S.C_e\right)^{1/n}} \quad (9)$$

$$\text{The Redlich} - \text{Peterson isotherm model } q_e = \frac{K_{RP} C_e}{1 + a_{RP} {C_e}^n} \quad (10)$$

Among these, q_e represents the quantity of hexavalent chromium (Cr (VI)) that is adsorbed by each unit of adsorbent mass, in milligrams per gram (mg/g). C_e, which denotes the concentrations of Cr(VI) remaining in the solutions at equilibrium, measured in milligrams per liter (mg/L). q_m is a critical parameter that indicates the maximum adsorption capacity of DE/Fe_3O_4/TSAC nanocomposite. K_L is the Langmuir constant related to energy (L/mg). K_f and n are unitless constants that correspond to the sorption capacity and intensity of adsorption, respectively. b is the adsorption heat (J/mol). K_T is the Temkin equilibrium binding constant (L/g). The temperature, denoted as T, is expressed in Kelvin, while R represents the universal gas constant with a value of 8.314 J/(mol·K). The parameters n_S (exponent of Sips; dimensionless), K_S (Sips constant, measured in L^n/mg^n), and a_{R-P} (measured in L/g) are determined through a non-linear fitting process.

In order to learn more about the properties of Cr(*VI*) sorption system, thermodynamic parameters such as the standard Gibbs free energy (ΔG°), standard entropy changes (ΔS°), and enthalpy changes (ΔH°) were computed by exploitation of Van't Hoff equation. For the adsorption of Cr(VI), the Gibbs free energy (ΔG°) in kJ·mol^{-1}, entropy (ΔS°) in kJ·mol^{-1} K^{-1}, and enthalpy (ΔH°) in kJ·mol^{-1} were calculated at thermodynamic equilibrium constants (Kc). The following is the adsorption's Gibbs free energy (ΔG):

$$(\Delta G^\circ) = (\Delta H^\circ) - (\Delta S^\circ) \quad (11)$$

where (ΔG°), obtained from Vant Hoff equations, is applied as follows.

$$(\Delta G^\circ) = -\text{RT ln Kc} \quad (12)$$

$$LnKc = (\Delta S^\circ)/R - (\Delta H^\circ)/RT \quad (13)$$

$$\text{Kc} = \text{dimentionless constand derived from isotherms} \quad (14)$$

where Kc is the equilibrium constant, M is the weight of the adsorbent in g·L^{-1}, V is the volume of solution in liters, and Co and Ce are the starting and equilibrium concentrations in mg·L^{-1}. The thermodynamic parameters, enthalpy (ΔH°), and standard adsorption entropy change (ΔS°) were obtained from slopes and y-intercepts, respectively, using the Van't Hoff linear plots of ln Kc against 1/T respectively.

2.6. Regeneration test

To assess the viability and affordability of the produced magnetic composite adsorbent, a regeneration test was carried out. The study began with the separation of a synthesized DE/Fe_3O_4/TSAC (MDA) composite from the solution mixture using magnet were presented in the supplementary material (Figure S_3). The recovered DE/Fe_3O_4/TSAC composite was then dried and soaked in a 0.1 M NaOH solution to reactivate the pores [3]. The suspension was agitated at 150 rpm for 45 min. Then, under ideal circumstances, the adsorbent was reused in the subsequent adsorption test after being cleaned with deionized water, isolated, and dried at 65 °C [9].

3. Result and discussion

3.1. Characterization studies

According to Fig. 2(a), the sulfuric acid treateddiatomite (TDE), teff straw activated carbon (TSAC), and magnetic composite adsorbent's (MDA). FTIR spectra of TDE show the characteristic peaks of amorphous silica. The intense peak at 1075.27 cm^{-1} (TDE) is due to Si-O-Si stretching vibrations. The minor shift and increased intensity in TDE are due to surface modification, enrichment of SiO_2, and removal of alkaline metallic impurities. Peaks at around 797.24 cm^{-1} (TDE) are assigned to Si-OH stretching, and peaks at around 457.15 cm^{-1} (TDE) are assigned to Si—O bond stretching. A new peak at 1180 cm^{-1} due to incorporated sulfate ions (SO_4^{2-}) as a result of sulfuric acid treatment in TDE [26,35]. FTIR spectrum of teff straw activated carbon (TSAC) shows some functional groups. The broad O—H stretching band at around 3400 cm^{-1}, which is prominent in teff straw due to the hydroxyl in hemicellulose and cellulose, decreases in TSAC, likely due to activation. C − H stretching (aliphatic C—H bonds) at 2920 cm^{-1} also decreases after activation. The band at 1740 cm^{-1} corresponds to aromatic C═C and carboxylic C═O stretching in both samples. Bands at around 1050 and 1150 cm^{-1} correspond to C-O-C bonds [36]. FT-IR spectra, the stretching vibrations of Fe-O-Fe are appeared by the usual absorption peak at 553.89 cm^{-1} [37,38]. Whilst the absorption peaks at 3331.83 and 1640 cm^{-1} are related to O—H stretching vibration of the silanol moiety within the silica in the diatomite [39]. Other absorption peaks observed at 803.54 cm^{-1} in the composite are related to Si—O stretching vibration on the silica shell [37]. With a carbonyl group present, the composite's absorption peak at 1066 cm^{-1} is assignable to C—O stretching vibration [40]. The peak at 2107.19 cm^{-1} may be responsible for C—H stretching vibrations [20]. The crystal structures of the the sulfuric acid treated diatomite (TDE), teff straw activated carbon (TSAC), and magnetic composite adsorbent's (MDA) were identified through XRD analysis as seen in Fig. 2(b). acid-treated diatomite (TDE) diatomite XRD patterns show broad peaks at 15°-30° 2θ, typical of amorphous silica. Consist of quartz and feldspar as major crystalline phases with minor amounts of cristobalite and montmorillonite. Notably, the montmorillonite peak at 2θ = 35° is absent in TDE due to leaching during H_2SO_4 treatment.

In the FTIR spectra of TSAC The intense background scattering in the XRD pattern between 19.47° and 32° 2θ is a sign that the carbon

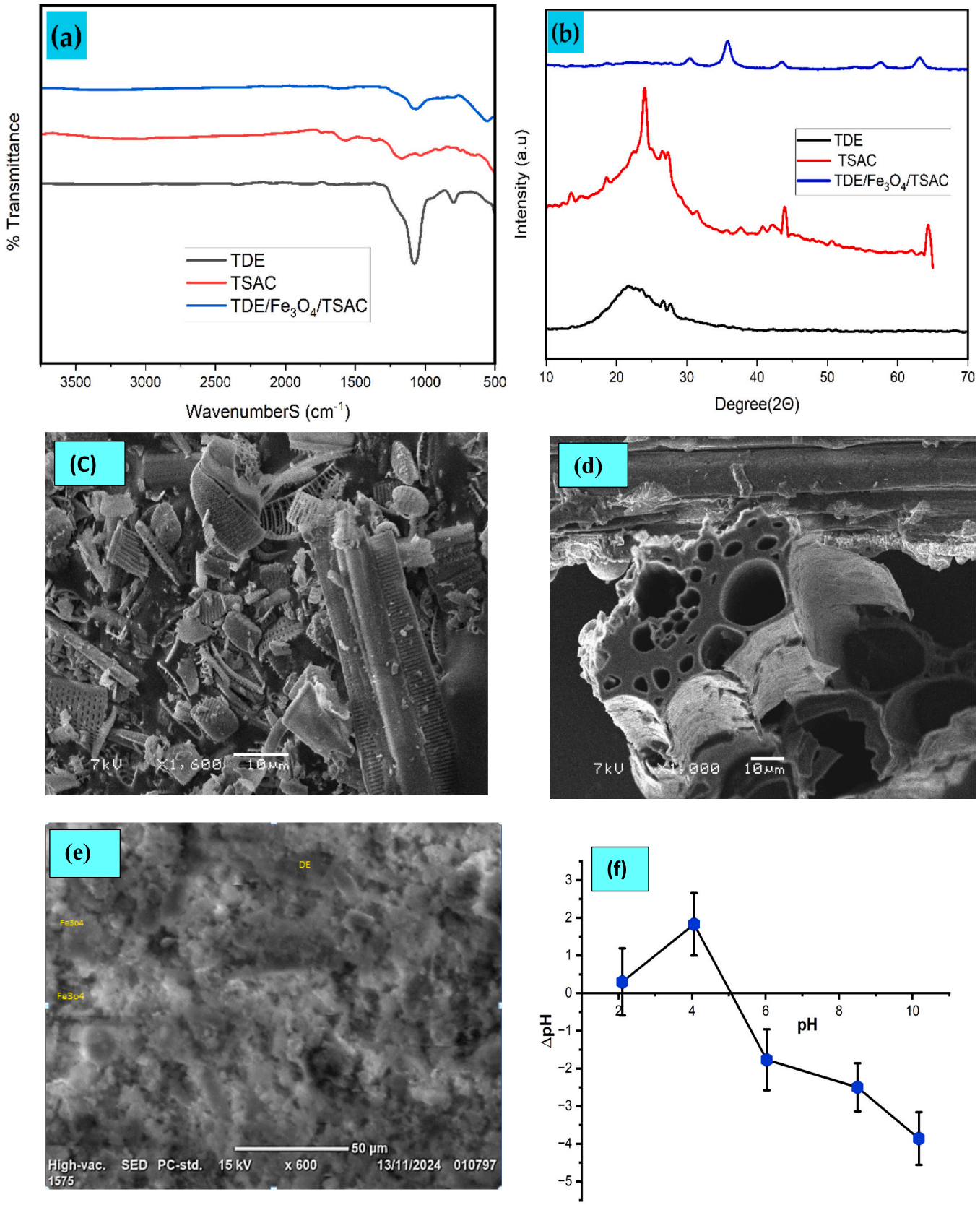

Fig. 2. FTIR spectra of TDE, TSAC, and DE/Fe_3O_4/TSAC. (a) spectrum of FTIR, (b) pattern of XRD, (c) SEM micrograph of TDE, (d) SEM micrograph of TSAC, (e) SEM micrograph of, DE/Fe_3O_4/TSAC, and (f) the graph of pH_{pzc} DE/Fe_3O_4/TSAC.

material either has a low crystallinity or very small crystal sizes, a common characteristic of activated carbons with their typical disordered structure. The existence of some crystalline order in the activated carbon is depicted by a small peak at 43.19° 2θ. The lack of intense, well-defined peaks in the XRD pattern indicates that there are no significant crystalline contaminants or inorganic materials present [28]. In the XRD of MDA, Diffraction peaks at 2θ = 30.5, 35.28, 42.5, and 63.16 were strongly linked to the typical patterns of FeO_4, [41,42]. These indicate the presence of a crystalline phase of Fe_3O_4 nanoparticles in the magnetic composites of diatomite, activated carbon, and magnetite. A minor peak is appeared at a 2θ of 26.6, which is associated with activated carbon [43] The weak peaks observed at low angles corresponding with the amorphous structure of SiO_2 [39]. These findings indicate that the synthesis of the magnetic composite adsorbent DE/Fe_3O_4/TSAC was successful. The sulfuric acid treated diatomite (TDE), teff straw activated carbon (TSAC), and the magnetic composite adsorbent of SEM image was presented in Fig. 2(c), (d) and (e) respectively. Acid treatment of diatomite (TDE) causes fracturing of the silica frustules, revealing the inner silica frameworks and hence the surface area of the material increases. Acid treatment also makes the pores within the diatomite particles larger, hence enhancing their adsorption capacities as shown in Fig. 2 (C). The SEM image in Fig. 2(d) shows TSAC has a highly porous structure with irregular micropores and mesopores, characteristic of activated carbons with high surface area for adsorption. This interconnected porosity and rough, heterogeneous surface with crevices likely result from the activation process, which creates pores and removes volatiles. The irregular particle shapes and sizes may contribute to the wide range of pore widths observed.

The morphological structure of the magnetic composite adsorbent was characterized by SEM. As shown in Fig. 2(c), most of the prepared DE/Fe_3O_4/TSAC consists of approximately spherical and uniform particles. This is due to the presence of a large number of sphere-shaped particles that form agglomerates with asymmetric distributions, resembling the characteristics of iron oxide magnetic nanoparticles. The prepared DE/Fe_3O_4/TSAC composite adsorbent exhibits a heterogeneous surface morphology characterized by rough and irregular features. The presence of Fe_3O_4 results in spherical particles, while the diatomite contributes elliptical and rod-like structures, similar to previous reports [44].

Exploiting the BET (Brunauer-Emmett-Teller) procedure, surface area of the prepared DE/Fe_3O_4/TSDAC was determined to be 347.458 m^2/g.

3.2. Adsorption result

3.2.1. Point of zero-point of charge (pHpzc)

The point of zero-charge of DE/Fe_3O_4/TSAC surface was computed to be at pH of 5, as shown in Fig. 2(f). When pHs are less than this value, the DE/Fe_3O_4/TSAC surface becomes protonated and positively charged, enhancing attraction toward negatively charged Cr(VI) species [45]. This increases the performance of Cr (VI) removal from aqueous solutions. Conversely, if solutions's pHs are higher than the zero-point charge pH, the surface becomes deprotonated (developing hydroxyl moieties), which leads to a reduced adsorption performance for Cr(VI) removal due to the repulsive forces between the DE/Fe_3O_4/TSAC surface and $HCrO_4^-$ and/or $Cr_2O_7^{2-}$ (Cr(VI) anions), thereby limiting the sorption process. Using the acid-base titration procedure was exploited to examine the synthesized materials' point of zero charge. The initial pH values is 2, 4, 6, 8, and 10 and After 48 h, the solution's pH was finally pH values obtained after titration 2.3, 5.93, 4.23, 5.5, and 6.14 was obtained respectively measured, and pH pzc was computed by overlapping the pH initial and pH final curves [30] as shown in Fig. 2(f). To ensure the reliability of our results, each experiment was conducted with a minimum of two repetitions.

3.2.2. Cr(VI) determination by UV–visible spectrophotometer

The UV–visible spectrophotometric approach was used to evaluate the produced composite adsorbents' ability to adsorb Cr(VI), with 1,5-DPC acting as a complexing agent [46]. The redox reaction betwixt Cr (VI) and DPC, in which DPC is oxidized to DPCO (diphenylcarbazone) and Cr (VI) is reduced to Cr(III), is what gives the pigment its pink-red hue [10] The calibration curve of concentration versus absorbance was created by measuring the absorbance of the working solutions.

3.3. Adsorption studies

Adsorption experiments were conducted on DE/Fe_3O_4/TSAC fabricated by different mixing ratios of 1.2: 0.4, 0.4:1.2, and 0.8:0.8 of TSAC to DE (*w*/w), as displayed in Fig. 3. The ratio of TSAC to DE significantly influenced both Cr(VI) removal efficiency and the resulting composite surface area. A1.2: 0.4 TSAC: DE ratio yielded 93.92 % Cr (VI) removal efficiency and surface area of 331.44 m^2/g. reversing the ratio to 0.4:1.2 resulted in a lower removal efficiency of 85.97 % and a smaller surface area of 173.187 m^2/g. the highest removal efficiency 98.96 % was achieved with a 0.8:0.8 TSAC:DE ratio, which also produced a high surface area of 347.458 m^2/g.

For this composite adsorbent, the effects of adsorption dosage, solution pH, adsorption period, and starting chromium ion concentration were examined.

3.3.1. Influences of adsorption variables

The effect of DE/Fe_3O_4/TSAC dosage on Cr(VI) removal efficacy was studied at adsorbent dosage of 0.01, 0.015, 0.02, 0.025, and 0.0.03 g/100 mL of the DE/Fe_3O_4/TSAC composite, yielding removal efficiencies of 87.45 %, 94.57 %, 96.15 %, 97.60 %, and 97.79.43 %, respectively as shown in Fig. 4 (a). DE/FeO_4/TSAC at a dose of 0.025 g/100 mL had the maximal sorption efficiency of 97.6 %. The composite adsorbent's effectiveness reaches a significant threshold at 0.025 g, after which additional augmentation results in decreasing removal efficiency; this plateau in removal efficiency indicates a saturation point, at which most of the adsorbent surface's active sites have already interacted with chromium ions; the observed phenomenon suggests that increasing the adsorbent quantity beyond this critical mass does not significantly improve the purification process. The complex interaction between the surface area of the adsorbent and the concentration of chromium ions in solution is responsible for this phenomenon. The likelihood of effective ion capture declines as the adsorbent gets closer to its maximum

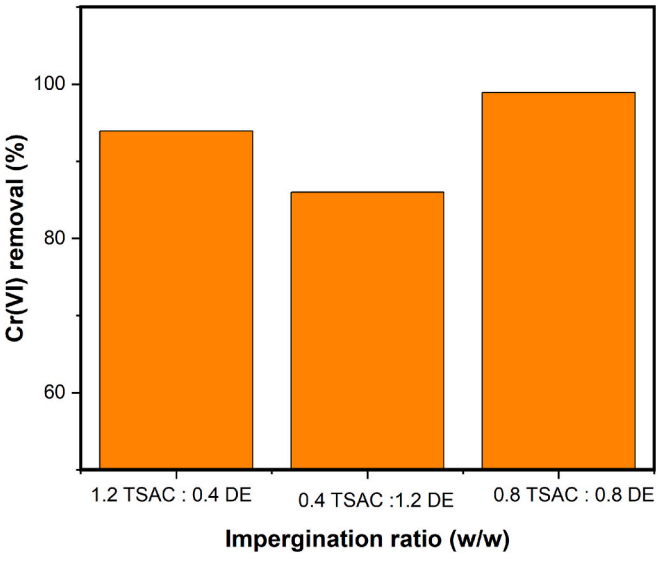

Fig. 3. Effect of impregnation ratio (weight of activated carbon to weight of diatomite) for preparation of DE/Fe_3O_4/TSAC on the Cr(VI) removal (%).

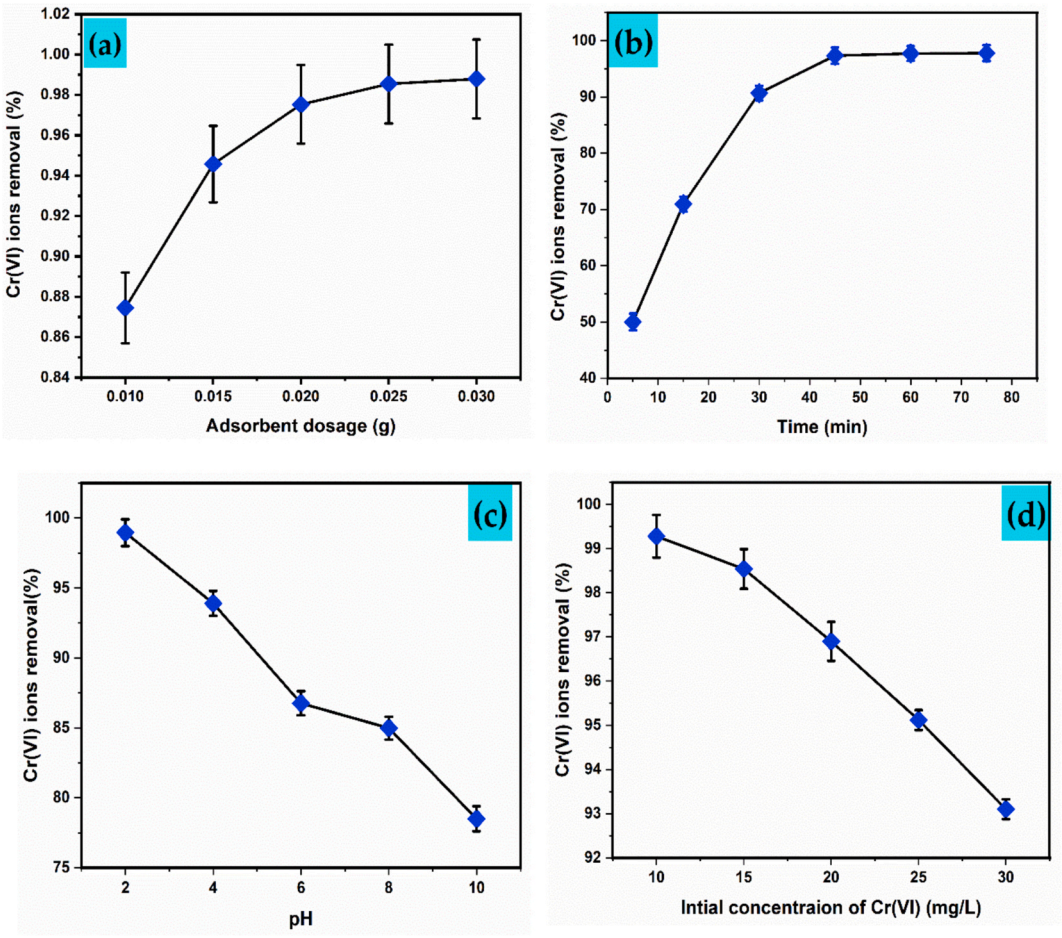

Fig. 4. The % removal effectiveness of Cr is influenced by adsorption settings. (a) adsorbent dosage, (b) sorption duration, (c) solution pH, and (d) initial Cr (VI) level.

capacity, leading to a very slight increase in removal efficiency overall. This knowledge is essential for maximizing the use of adsorbents while striking a balance between material consumption and treatment efficacy [20].

By adjusting the contact period from 15 to 75 min, the impact of contact duration on the DE/FeO_4/TSAC composite's ability to remove Cr (VI) was examined [47]. The adsorption of Cr(VI) by the DE/Fe_3O_4/TSAC composite occurred rapidly in the initial minutes due to the abundance of available unsaturated sites on the surface as demonstrated in Fig. 4(b). However, the adsorption slowed down later, likely due to the heterogeneous nature of the synthesized adsorbent [48].

As the contact time extended to 45 min, the adsorption efficiency improved, reaching 97.33 % for Cr (VI) removal; the adsorbate had more opportunities to diffuse onto the adsorbent sites [49]. By adjusting the pH values 2, 4, 6, 8, and 10 under specific conditions, the influence of pH on Cr(VI) removal by DE/Fe_3O_4/TSAC composite was investigated. The removal efficiency declines from 2 to 10. In acidified solution pHs, the positively charged surface of the DE/Fe_3O_4/TSAC composite shows strong electrostatic attraction with the negatively charged $HCrO_4^-$ and $Cr_2O_7^{2-}$ pollutants [49]. Chromium VI is effectively reduced to chromium III, a less hazardous and more stable oxidation state, in an acidic environment. The redox reaction can be expressed as $HCrO_4^- + Fe^{2+} + 7H^+ \rightarrow Cr^{3+} + Fe^{3+} + 4H_2O$ [47]. Due to the better adsorption properties of the DE/FeO_4/TSAC composite toward Cr(III) ions, this conversion increases the removal efficiency of chromium species. The procedure, which is depicted in the reaction that goes along with it, shows how surface contacts and redox chemistry work in concert to remediate heavy metals. Above pH 5, the DE/Fe_3O_4/TSAC composite's surface becomes negatively charged as shown in Fig.4(c), causing repulsion with the negatively charged chromium anions. Under alkaline conditions, chromate ions (CrO_4^{2-}) dominate as the principal hexavalent chromium species, engendering a competitive adsorption dynamic wherein CrO_4^{2-} and hydroxyl anions (OH^-) vie for occupancy of active surface sites [48]. Such a competition would decline the adsorption of hexavalent chromium.

As can be grasped from the results, in summary, adsorption efficiency decreased from 98.95 to 78.50 % when the pH rose from 2 to 10. As the initial Cr(VI) level rose from 10 to 30 mg/L, the DE/Fe_3O_4/TSAC composite's adsorption efficiency first dropped from 99.28 % to 91.1 2 %, as illustrated in Fig. 4(d). At first, the observed adsorption efficiency of Cr(VI) on DE/Fe3O4/TSAC shows good performance, which is mechanistically explained by the huge number of unoccupied active sites on the surface of the composite [8], which provides strong affinity toward the pollutant. However, as Cr(VI) concentrations increase, the system's removal capacity decreases [50], mainly because of two synergistic factors: (i) site saturation, as progressive occupation of surface-active centers reduces available binding domains, and [7] inter-adsorbate interference, as increased ionic crowding induces competitive interactions between adsorbate species, destabilizing adsorption equilibria through steric hindrance and electrostatic repulsion impacts.

3.3.2. Experimental design and statistical analyses

Through response surface methodology (RSM) utilizing a central composite design (CCD) framework, the optimization and interactive effects of critical adsorption parameters, specifically adsorbent dosage (A), solution pH (B), contact time (C), and initial Cr(VI) level (D), were

thoroughly examined. This allowed for a methodical assessment of the influences of individual factors and multivariate interactions governing the efficiency of the sorption process.150 rpm was the agitation pace at which the mixing occurred. The impacts of the four parameters are displayed in Table 2, along with the corresponding removal percentage of Cr (VI) ions as determined experimentally and projected.

A polynomial expression (second-order) was exploited to characterize the relationships betwixt the four independent parameters and removal percentages of Cr (VI) ions (response).

The constructed model has a strong fit, as recognized by its R^2 (coefficient of correlation) of 0.9816. The ANOVA (analysis of variance), model fit and summary statistics, and the experimental design matrix generated by CCD for Cr(VI) ions removal of the founded model were not shown here.

The terms in the model are significant, according to the *p*-value, which is less than 0.05. Given that their *p*-values are lower than 0.05, the terms A, B, C, D, AC, B^2, C^2, and D^2 are significant. Eq. 16 illustrates the empirical relationship between the input variables and removal efficiency percentage of Cr(VI) ions as the response variable.

$$\mathbf{R}\ (\%) = \mathbf{83.90} + \mathbf{1.6\ A} + \mathbf{3.16\ B} - \mathbf{4.82\ C} - \mathbf{2.65\ D} - \mathbf{0.4575\ AB} + \mathbf{0.8575\ AC} + \mathbf{0.5575\ AD} - \mathbf{0.5550\ BC} - \mathbf{0.4550\ BD} + \mathbf{0.4825\ CD} - \mathbf{0.2344\ A^2} - \mathbf{1.80\ B^2} + \mathbf{1.06\ C^2} - \mathbf{0.5269 D^2} \quad (16)$$

3.3.2.1. ANOVA for the quadratic model. For statistical analysis of input effective variables (A, B, C, D) and for empirical model validation purposes, certain parameters were considered. Analysis of variance (ANOVA) is a technique used to determine validity and adequacy of the models through Fisher's, F-test, and Student's *t*-test. In this case, F-values and P-values suggest the design factors, adsorbent dose, contact time, pH, and, initial Cr (VI) concentration, are highly significant for the quadratic model. The Cr (VI) adsorption removal responses of the experimental design show optimal conditions at adsorbent dose = 0.024, time 59.99, pH = 4, initial Cr (VI) concentration 15 mg/L with 94.83 % removal efficiency.

Table 2
Experimental design matrix generated by CCD for Cr (VI) ion removal.

Run	Factors				Cr(VI) ions removal percentage (%)	
	A	B	C	D	Experimental	Predicted
1	0.02	30	8	15	74.80	74.33
2	0.04	30	8	15	77.80	79.04
3	0.04	30	4	15	86.80	86.81
4	0.03	45	6	20	83.90	83.90
5	0.04	60	4	25	87.80	88.19
6	0.03	45	6	20	83.90	83.90
7	0.03	45	10	20	78.50	78.51
8	0.03	45	6	10	86.70	87.09
9	0.02	60	4	15	93.50	94.80
10	0.02	60	4	25	86.50	86.51
11	0.05	45	6	20	87.50	86.16
12	0.04	60	8	15	84.90	84.25
13	0.03	45	6	20	83.90	83.90
14	0.04	30	4	25	80.80	82.58
15	0.02	60	8	15	81.90	81.38
16	0.03	45	6	20	83.90	83.90
17	0.01	45	6	20	79.60	79.77
18	0.03	45	6	20	83.90	83.90
19	0.02	60	8	25	75.11	75.02
20	0.02	30	4	15	86.40	85.54
21	0.04	60	4	15	93.90	94.25
22	0.03	75	6	20	83.90	83.04
23	0.03	45	6	30	78.06	76.50
24	0.02	30	8	25	68.89	69.80
25	0.04	30	8	25	78.11	76.74
26	0.03	15	6	20	70.70	70.39
27	0.04	60	8	25	78.01	80.13
28	0.03	45	6	20	83.90	83.90
29	0.03	45	2	20	98.95	97.77
30	0.02	30	4	25	78.50	79.07

The model test demonstrates that the design model accurately depicts the data behaviour for the experiments and the considered factors have extremely significant effects on removal efficiency [51]. The model optimized for Cr (VI) removal by the CCD suggested a quadratic model, with regression and adjusted regression (R^2) values of 0.8941 and 0.9644, respectively, as shown in Table 3. The model is acceptable if R^2 approaches unity [52]. These parameters have incredibly large effects on removal efficiency.

In general, to validate this empirical model, several parameters were considered, such as probability <0.05 would show the significance of the model and lack of fit should be not significant (> 0.05), and adequate precision (signal-to-noise ratio) is >4, as shown in Table 4.

the Residual plots, and normal probability plots as shown Fig. 5.

The three-dimensional response surface analysis (Fig. 6) shows important synergistic interactions between process variables in the removal efficiency of chromium (VI). In particular, Fig. 6(a) shows that the adsorbent dosage (Factor A) and contact time (Factor B) have a codependent relationship, with the lowest removal efficiencies occurring at minimal adsorbent dosages and shorter contact times.

The impacts of solution pH (C) and dose (A) on sorption efficiency of Cr(VI) are displayed in Fig. 6(b). As the pH of the solution drops and the sorbent dosage is increased, the removal efficiency of Cr(VI) rises. Higher solution pH and lower adsorbent dosage resulted in the lowest removal effectiveness. In general, a higher adsorbent dosage and a comparatively lower pH produced the highest removal %. A 3D figure showing the impact of the starting concentration of Cr(VI) and DE/Fe_3O_4/TSAC dose (A) upon sorption efficiency of Cr(VI) from aqueous water is demonstrated in Fig. 6(c). As the starting concentration decreases and the adsorbent dosage increases, the removal efficiency rises. Fig. 6(d) illustrates the combined impact of contact duration (B) and solution pH (c). Its removal efficacy response rises as the solution's pH falls and contact time lengthens. However, as the starting concentration rises, the effectiveness of chromium removal falls.

Fig. 6(e) showed how initial Cr(VI) level and contact duration interacted. While the removal efficiency rises with contact duration, it falls with increasing initial Cr(VI) level. Fig. 6(f) showed the combined impact of the initial Cr (VI) level and solution pH (C). It demonstrates that as the starting Cr(VI) level and medium's pH both drop, the removal efficiency rises.

An optimal Cr (VI) ion's removal of 94.83 % was attained using the response surface technique model at the following parameters: initial Chromium (VI) level (15 mg L-1), contact duration (59.99 min), DE/Fe_3O_4/TSAC dose (0.024 g), and solution pH (4). A set of duplicate tests were conducted underneath the determined ideal conditions in order to verify the optimization outcomes acquired from the CCD-based RSM model. At a sorbent dose of 0.024 g, solution pH of 4, beginning Cr(VI) concentration of 15 mg/L, and contact time of 59.99 min, the experimental removal efficiency of Cr(VI) was grasped to be 93.28 ± 1.22 %. The strong correlation betwixt the predicted amounts and the experimental results highlights how accurate and dependable the created model is at predicting the removal efficiency of Cr(VI) from aqueous solutions by exploitation of the magnetic composite adsorbent.

3.3.3. Adsorption isotherm study

The data of equilibrium experiments were subjected to the Langmuir, Freundlich, Temkin, and three three-parameter isotherm models in order to analyse the adsorption mechanism and ascertain the maximum.

The DE/Fe_3O_4/TSAC composite adsorbent's adsorption capacity was assessed, and isotherm models were used to examine the adsorption behaviour. The study determined the isotherm model that best explains the experimental adsorption data by evaluating the coefficient of determination (R^2), offering a reliable explanation of the adsorption mechanism. In order to achieve this, Cr(VI) adsorption isotherm experiments were carried out using 100 mL solution and agitation speed =

Table 3
Model fit and summary statistics.

Source	Std. Dev.	R^2	Adjusted R^2	Predicted R^2	PRESS	
Linear	2.81	0.8388	0.8130	0.7516	303.95	
2FI	2.95	0.8650	0.7939	0.7273	333.71	
Quadratic	**1.22**	**0.9816**	**0.9644**	**0.8941**	**129.63**	**Suggested**
Cubic	0.9189	0.9952	0.9800	0.3043	851.15	Aliased
		Coefficient of variance	1.48		Adequate precision	32.2955

Table 4
ANOVA of the second order polynomial equation.

Source	Sum of Squares	df	Mean Square	F-value	p-value	
Model	1201.03	14	85.79	57.18	< 0.0001	significant
A-Dose	61.18	1	61.18	40.78	< 0.0001	
B-Time	240.16	1	240.16	160.07	< 0.0001	
C-pH	556.61	1	556.61	370.99	< 0.0001	
D-Intial Con	168.33	1	168.33	112.19	< 0.0001	
AB	3.35	1	3.35	2.23	0.1559	
AC	11.76	1	11.76	7.84	0.0135	
AD	4.97	1	4.97	3.31	0.0887	
BC	4.93	1	4.93	3.28	0.0900	
BD	3.31	1	3.31	2.21	0.1580	
CD	3.72	1	3.72	2.48	0.1360	
A^2	1.51	1	1.51	1.00	0.3322	
B^2	88.56	1	88.56	59.03	< 0.0001	
C^2	30.78	1	30.78	20.52	0.0004	
D^2	7.61	1	7.61	5.07	0.0397	
Residual	22.51	15	1.50			
Lack of Fit	22.51	10	2.25			
Pure Error	0.0000	5	0.0000			
Cor Total	1223.53	29				

150 rpm. The initial level was varied from 10 to 40 mg/L whilst keeping pH at 4, the adsorption time was 60 min, the temperature was 25 °C, and the adsorbent dosage was 0.024 g (parameters at optimal levels). The models used for equilibrium sorption data, as displayed in Fig. 7 (a) an reported in Table 5, to determine if these models effectively describe the adsorption process. When compared to the theoretical model of monolayer adsorption on heterogeneous surfaces, the equilibrium data analysis provides detailed information about the adsorption mechanism [47]. The isotherms which had three parameters showed a good statistical coherence among the models evaluated, with an R^2 values larger than 0.9955 and low error metrics (ARE≤0.081 %, Δq ≤ 3.73 %, $\chi^2 \leq$ 0.397), which is consistent with the Langmuir-based theory of monolayer adsorption [48], since such models naturally reduces to the Langmuir equation when its heterogeneity parameter (n) approaches unity [49]. Although the observed deviation of n from 1 suggests surface energy heterogeneity, the Redlich-Peterson model further supports the dominance of monolayer behaviour with suitable goodness-of-fit (R^2 = 0.9977) and hybrid features of Langmuir and Freundlich mechanisms. Crucially, while site-specific energies were constant, the Langmuir isotherm itself maintained strong validity (R^2 = 0.9925), which is consistent with its ability to explain heterogeneous but localized monolayer adsorption. The Temkin model's poorer performance (R^2 = 0.9540) and the Freundlich isotherm's intermediate findings (R^2 = 0.9872) indicate that although surface heterogeneity affects adsorption energetics, the monolayer assumption is still true. The Tóth model was assessed in the dataset and showed a good fitness with the data, resolving this contradiction by theoretically extending Langmuir's framework to measure energy distribution heterogeneity while maintaining monolayer adherence [50]. This is a natural expansion considering the trends in the data that have been seen. The remarkable accuracy of Langmuir and the convergence of models with three parameters (Sips, Tóth, and Redlich-Peterson) highlight a hybrid mechanism: monolayer adsorption on a surface with moderate energy heterogeneity. By taking into account adsorption site variability, three-parameter models enhance rather than replace the monolayer paradigm, which is why this interpretation disproves the multilayer conclusion from Freundlich intermediate alignment. Accordingly, the system is best characterized as a heterogeneous monolayer process, in which Langmuir is still essentially valid under its localized-site assumptions.

3.3.4. *Adsorption kinetics study*

Through batch experiments using 100-mL of aqueous solutions with

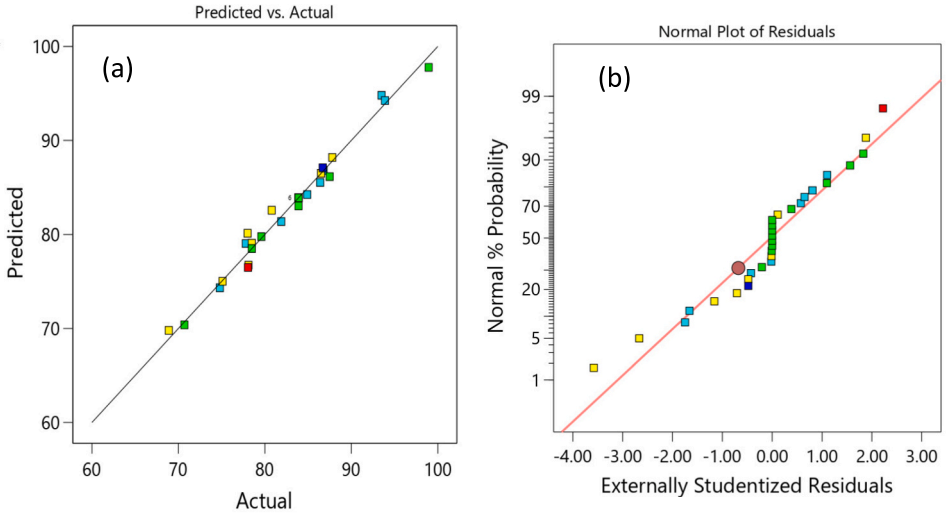

Fig. 5. The graphical illustration for the predicted and actual Cr (VI) removal efficiency (a). The graphical illustration for the normal plot of Residuals (b).

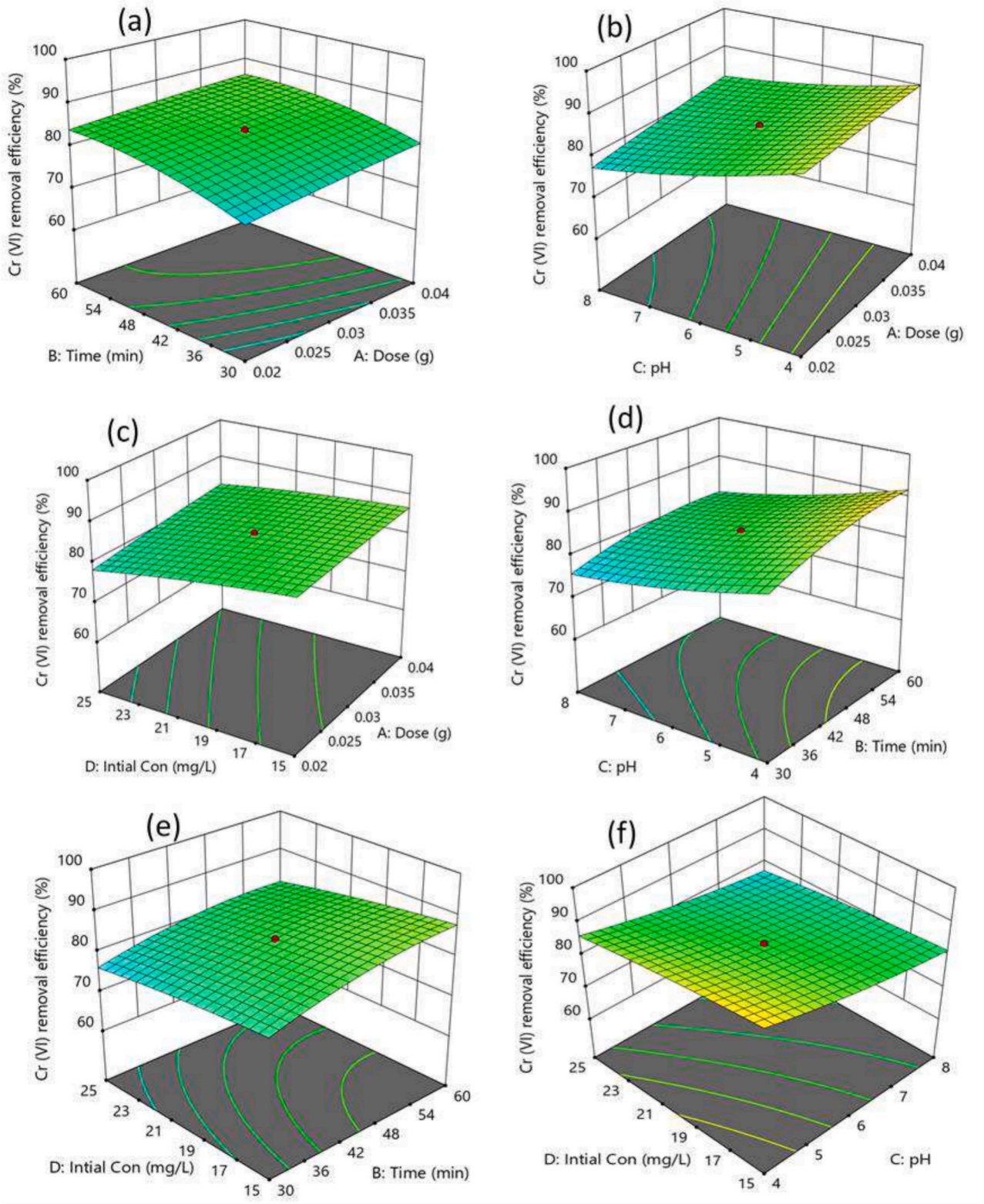

Fig. 6. 3-D surface graphs showing how the adsorption parameters interact.

an initial chromium concentration of 15.0 mg/L and 0.024 g of DE/Fe3O4/TSAC at pH 4.0 and 25 °C, the sorption kinetics of Cr(VI) were systematically investigated. The rate-limiting processes were interpreted using three mechanistic models: pseudo-first-order (PFO), pseudo-second-order (PSO), and intraparticle diffusion (IPD). Kinetic analysis showed superior alignment with the PSO model ($R^2 > 0.99$), Table 6, resulting in an equilibrium adsorption capacity (q_e) of 63.05 mg/g. Although, based some published work in the literature [51], this significant association indicates that chemisorption is the dominant mechanism, a chemisorption cannot be at play in the current adsorption system. In fact, a chemisorption process is most likely due to covalent electron transfer between the active surface sites on the DE/Fe_3O_4/TSAC

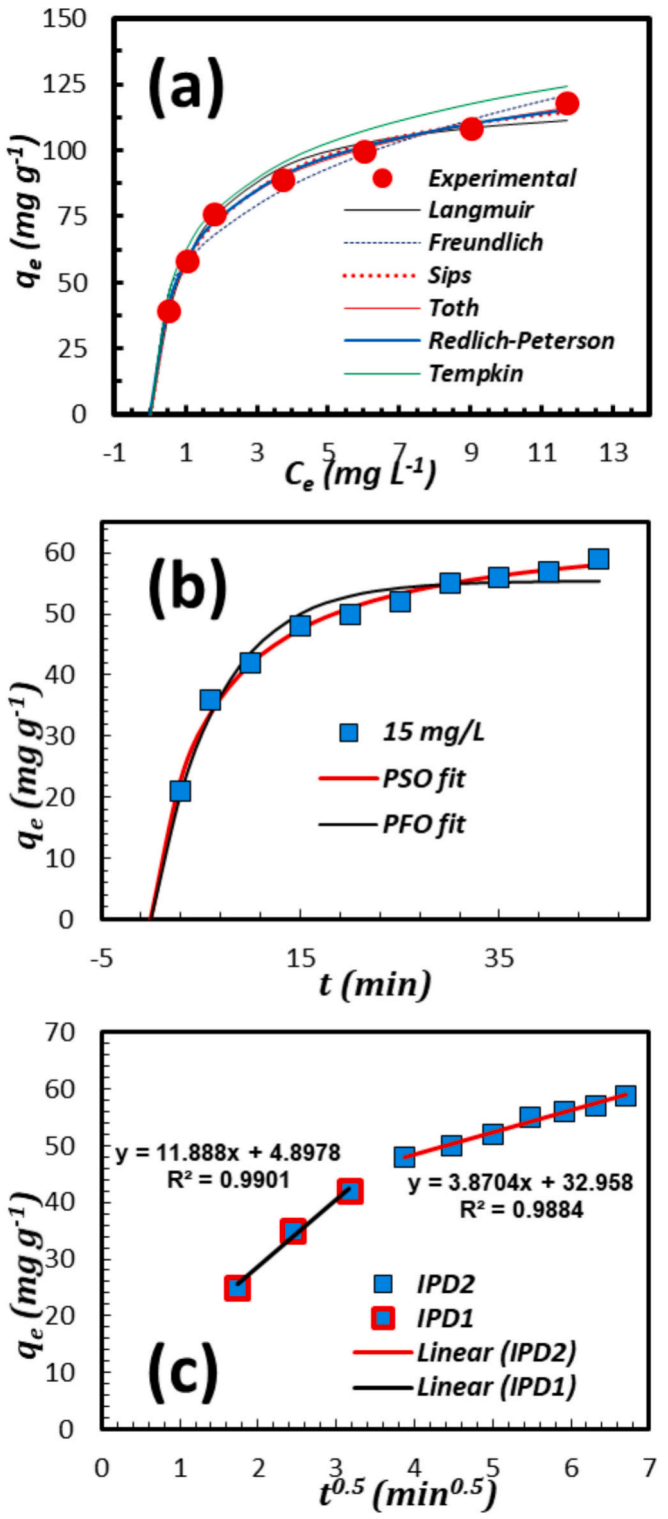

Fig. 7. Plots of various isothermal models (a), various kinetic models (b), and intra-particle model (c).

and Cr(VI) oxyanions [53]. However, the possibility of such process is quite low in DE/Fe_3O_4/TSAC and Cr(VI) system. With high intercept values (C) in multilinear regression plots, the IPD model showed an acceptable applicability ($R^2 \geq 0.9884$). However, the defined stages show a high intercept which suggests that boundary layer effects were a main resistance mechanism throughout the examined period, surpassing pore diffusion. Together, our results support the idea that surface complexation, not physical mass transfer limitations, controls adsorption kinetics. This is in line with physiochemical-mediated removal mechanisms that have been documented for similar sorption systems [49].

3.3.5. Thermodynamics

Using linear van't Hoff analysis, the thermodynamic parameters controlling the process were identified [53]. The temperature-dependent equilibrium data were fitted to the formula ln(numerical value of K_L(L/mol) $= -\Delta H^{\circ}/RT + \Delta S^{\circ}/R$. The slope of −4497 and the intercept of 28.142 obtained from linear regression of ln(numerical value of K_L(L/mol) versus 1/T (Fig. 8) equate to an entropy change (ΔS∘) of 186.41 J/(mol.K) and an enthalpy change (ΔH°) of 36.06 kJ/mol. While the positive ΔS∘ indicates increasing molecular disorder at the solid-liquid interface during the process, the positive ΔH∘ validates the andothermic character of Cr(VI) adsorption onto DE/Fe_3O_4/TSAC. The consistently negative Gibbs free energy values (ΔG∘) demonstrated the spontaneity of adsorption; they varied from −31.20 kJ/mol at 20° to −34.66 kJ/mol at 35 °C. According to the Gibbs-Helmholtz relationship $\Delta G^{\circ} = \Delta H^{\circ} - T\Delta S^{\circ}$, this pattern is consistent with the enthalpy-driven contribution, which is more prominent at higher temperatures and less so as thermal energy decreases. In line with the endothermic adsorption mechanism, the gradual increase in ΔG∘ negativity over the studied temperature range (20–35 °C) indicates raised thermodynamic favorability at higher temperatures [49].

3.3.6. Regeneration test

The regeneration capability of an efficient adsorbent and the safe disposal of wastewater are crucial factors in assessing its economic feasibility [54]. As shown in the Fig. 9, the adsorption efficiency of DE/Fe_3O_4/TSAC after each cycle. The recyclability of DE/Fe_3O_4/TSAC demonstrated excellent performance for five consecutive cycles, with adsorption efficiency of that is 93.26, 88.12, 84.15, 78.59, and 74.02 % for first, second, third, fourth, and fifth runs, respectively. Indeed, the sorption efficacy demonstrated a slight decline, as displayed Fig. 8. According to the pseudo-second-order model, this might be explained by closes of some pores by participated pollutant. This suggested that DE/Fe_3O_4/ TSAC composite adsorbent is a promising and cost-effective for the adsorption of Cr(VI), making this sorbent suitable for practical applications.

3.3.7. Comparison of DE/Fe_3O_4/TSAC with adsorptive removal of Cr (VI) for clay composite

The exceptional stability, cost-effectiveness, and high adsorption potential of clay-based composites have attracted a lot of attention. Of these, the DE/Fe_3O_4/TSAC composite showed an excellent maximum adsorption capacity of 131.01 mg/g for Cr(VI), which is attributed to the electrostatic interactions between negatively charged Cr(VI) anionic species and the positively charged surface of DE/Fe_3O_4/TSAC under ideal conditions. Table 7 summarizes comparative analyses of different clay-based composite adsorbents, highlighting the superior adsorption efficiency and efficacy of DE/Fe_3O_4/TSAC in removing heavy metal pollutants. Its potential as a sustainable wastewater treatment solution is further highlighted by the fact that it is made from cheap, plentiful clay minerals and teff straw obtained from biomass. Additionally, DE/FeO_4/TSAC's magnetic characteristics make it simple to separate from aqueous solutions with the use of an external magnetic field, allowing for effective regeneration and reuse. Because of these qualities, DE/FeO_4/TSAC is positioned as a viable option for developing environmentally friendly water treatment systems. The comparative removal capacity study of Cr(VI) removal indicates the remarkable enhancement attained with the ternary composite (TDE/Fe_3O_4/TSAC. relative to individual counterparts and even certain reported binary systems. Whereas H_2SO_4 treated diatomite and teff straw activated carbon had capacities of 16.39 mg/g [26]and 49.285 mg/g [28], respectively, their coupling with Fe_3O_4 in the TDE/Fe_3O_4/TSAC composite enhanced the Cr removal exponentially to a peak of 131.01 mg/g. This is well beyond the

Table 5
Isotherms constants for uptake of Cr(VI) on DE/Fe_3O_4/TSAC.

Models	Equations	Parameter		Statistical indices				
Langmuir's Isotherm	$q_e = \frac{q_m K_L C_e}{1 + K_L C_e}$	q_m (mg/g)	K_L (L/mg)	R^2	Δq	χ^2	ARE	
		131.019	0.892	0.9925	4.013	0.839	0.161	
Freundlich's isotherm	$q_e = K_f C_e^{\frac{1}{n}}$	K_f (L/g)	n	R^2	Δq	χ^2	ARE	
		57.01	3.27	0.9872	6.267	1.916	0.483	
Temkin's isotherm	$q_e = \frac{RT}{b}(\ln K_T C_e)$	K_T (L/g)	b (J/mol)	R^2	Δq	χ^2	ARE	
		12.01	25.10	0.9540	10.975	3.56	1.012	
Sips's isotherm	$q_e = \frac{q_m (K_S C_e)^{1/n}}{1 + (K_S C_e)^{1/n}}$	q_m (mg/g)	n	K_s (L/g)	R^2	Δq	χ^2	ARE
		140.31	1.31	0.61	0.9955	3.73	0.397	0.079
Redlich- Peterson's isotherm	$q_e = \frac{K_{RP} C_e}{1 + a_{RP} C_e^{\,n}}$	K_{RP} (L/g)	n	a_{RP} (L^n/mg^{-n})	R^2	Δq	χ^2	ARE
		150.96	0.881	1.63	0.9977	3.233	0.381	0.081
Tóth's isotherm	$q_e = \frac{q_{max} K_T C_e}{[1 + (K_T C_e)^n]^{1/n}}$	K_T (mg/L)	n	q_{max} (mg/g)	R^2	Δq	χ^2	ARE
		1.52	0.52	135.03	0.9985	2.93	0.199	0.048

Table 6
Models' constants for sorption kinetics for Cr (VI) on DE/Fe_3O_4/TSAC.

Models	Equations	Parameter			Statistical indices		
PFO	$q_t = q_{e1}\left[1 - exp^{(-k_1 t)}\right]$	q_{e1} in mg/g	k_1 in 1/min	R^2	Δq	χ^2	ARE
		55.49	0.16	0.9459	7.10	1.67	0.50
PSO	$q_t = \frac{q_{e2}^2 k_2 t}{[k_2 q_{e2} t + 1]}$	q_{e2} in mg/g	k_2 in g/mg min	R^2	Δq	χ^2	ARE
		63.05	0.0027	0.9902	3.59	0.37	0.13
IPD1 & IPD2	$q_t = k_p t^{0.5} + c$	$k_{p,1}$ in mg/g $min^{0.5}$	C in mg/g	R^2	$k_{p,2}$ in mg/g $min^{0.5}$	C in mg/g	R^2
		11.89	4.90	0.9901	3.87	32.96	0.9884

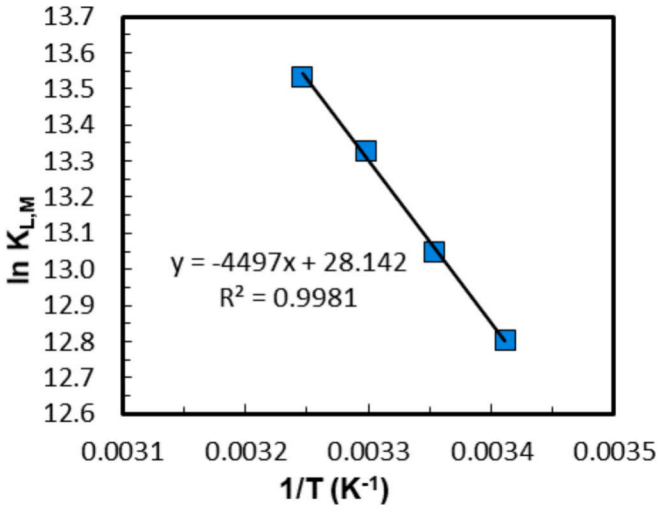

Fig. 8. The Adsorption data is plotted as $\ln K_c$ (ln(numerical value of K_L in L/mol) against (1/T).

capacities of the other materials considered here, such as magnetite diatomite (88.49 mg/g) [25], montmorillonite clay-supported magnetite nanoparticles (15.3 mg/g), and surfactant-modified montmorillonite clay (41.34 mg/g) [55] Such a dramatic enhancement of the Cr (VI) adsorption capacity of the ternary composite, especially compared to its constituent parts and binary analogs, indicates a profound synergistic effect in which the integration of Fe_3O_4 with the modified diatomite and activated carbon develops a more effective adsorption platform. This higher performance can likely be attributed to the synergistic effects of the porous structure and high surface area of the activated carbon and diatomite, the acid functional groups from the sulfuric acid treatment of diatomite and nitric acid oxidation of activated carbon, and the magnetism and potential Cr(VI) reduction capacity of the Fe_3O_4, as seen from various studies on similar magnetic composites for heavy metal removal [25].

3.3.8. *Mechanism of Cr(VI) sorption*

The sorption of Cr (VI) onto the surface of fabricated DE/Fe_3O_4/TSAC composite may occur through mechanisms such as electrostatic interaction [60], chelation, H-bonding, surface precipitation [14], or reduction-adsorption processes (Fig. 10). The potential removal of Cr (VI) from aqueous solutions can involve formation of complexes and precipitation at the surface [13]. This could be because the surface of the produced DE/Fe_3O_4/TSAC composite has enhanced functional groups. The conversion of Cr(VI) to Cr(III), which is then eliminated via adsorption, is another possible adsorption mechanism [6]. In acidified solution pHs, the positively charged surface of the DE/Fe_3O_4/TSAC composite shows strong electrostatic attraction with the negatively charged $HCrO_4^-$ and $Cr_2O_7^{2-}$ pollutants [49]. Chromium VI can effectively be reduced to chromium III, a less hazardous and more stable oxidation state, in an acidic environment. From thermodynamic studies, the magnitude has been found to be 36.06 kJ/mol, which is far higher than ΔH° range of physiosorption processes (i.e., approximately 2.0 to 20 kJ/mol [61]). This high ΔH° magnitude can be due to association a chemical process (like reduction of Cr(VI) to Cr(III)) which may be at play for a part of Cr(VI) amount which is adsorbed on the surface of adsorbent. In fact, perhaps due to the better adsorption properties of the DE/FeO_4/TSAC composite toward Cr(III) ions, this conversion increases the removal efficiency of chromium species. The procedure, which is depicted in the reaction that goes along with it, shows how surface contacts and redox chemistry work in concert to remediate heavy metals. Above pH 5, the DE/Fe_3O_4/TSAC composite's surface becomes negatively charged as shown in Fig. 2(f), causing repulsion with the

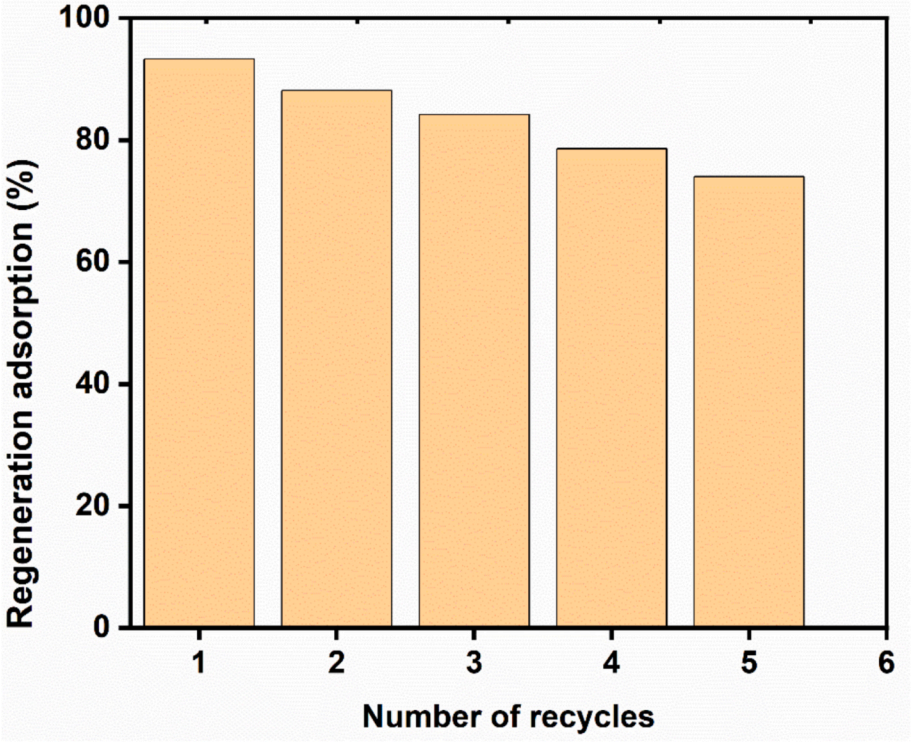

Fig. 9. Reusability test of DE/Fe_3O_4/TSAC composite.

Table 7
Comparing the capability of the DE/Fe_3O_4/TSAC adsorbent to that of other clay-based composite sorbents for the removal of Cr(VI).

Clay-based composite	Percent (%) removal maxmuim adsorption capacity(mg/g)	Isotherm model	Kinetic model (Pseudo)	Reference
Magnetic- bentonite	96.84 %	Tempkin	1st	[56]
Carbon–diatomite	19.91 mg/g	Langmuir	2nd	[57]
Chitosan-coated bentonite clay	106.444 mg/g	Dubinin Radushkevich	–	[58]
Kaolinite–Fe/Al oxide (hydroxide)	70.71 mg/g	Langmuir	–	[59]
Magnetic zeolite	43.93 mg/g	–	1st	[1]
Magnetite diatomite	88.49 mg/g	Langmuir & Freundlich	2nd	[25]
Montmorillonite clay-supported magnetite nanoparticles	15.3 mg/g	–	–	[55]
Polyethylenimine functionalized magnetic montmorillonite clay	62.89	–	–	[55]
H_2SO_4 treated diatomite	16.39 mg/g	Freundlich	–	[26]
Teff straw activated carbon	49.285 mg/g	Langmuir & Freundlich	2nd	[28]
TDE/Fe_3O_4/TSAC	131.01 mg/g	–	–	This study

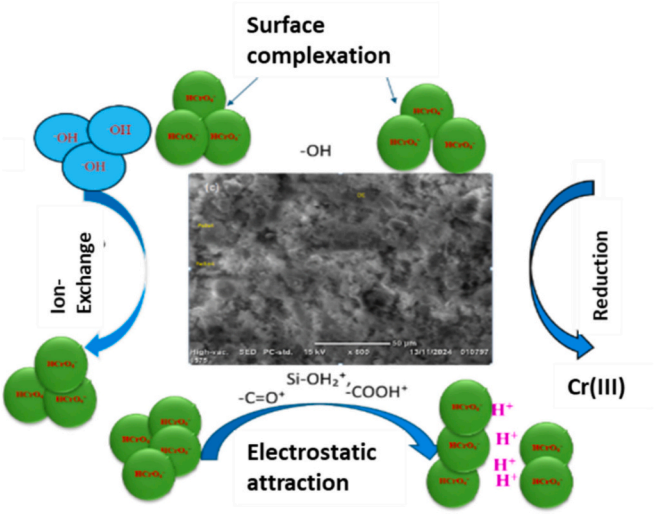

Fig. 10. Adsorption mechanism of Cr(VI) on the surface of synthesized TDE/Fe_3O_4/TSAC adsorbent.

negatively charged chromium anions. Under alkaline conditions, chromate ions (CrO_4^{2-}) dominate as the principal hexavalent chromium species, engendering a competitive adsorption dynamic wherein CrO_4^{2-} and hydroxyl anions (OH^-) vie for occupancy of active surface sites [48]. Such a competition would decline the adsorption of hexavalent chromium.

4. Conclusion

In this study, DE/Fe_3O_4/TSAC composite was synthesized from precursors (DE, Fe_3O_4, and TSAC), its characterization was carried out, and examined for their ability for adsorption of Cr(VI) from aqueous media. To construct a magnetic composite adsorbent, the impact of the adsorption of Cr(VI) removal was appraised using the impregnation ratio (weight of TSAC: weight of DE). The synthesized composite adsorbent generated under maximal impregnation ratio conditions was characterized, exploiting FTIR, SEM, XRD, and BET. The DE/Fe3O4/TSAC was found to have a microporous structure with a BET surface area of 347.45 m^2/g. The composite adsorbent's pH pzc was found to be 5, meaning that its surface is negatively charged at pH levels higher than 5 and positively charged at pHs below 5. Findings affirmed the presence of significant active sites and functional moieties that may resemble the properties of the composite adsorbent noted in other studies. Using RSM (response surface methodology) with CCD, the impact of adsorption factors (solution pH, adsorbent dosage, initial Cr(VI) level, and adsorption period) on the chromium removal % was investigated. At solution pH (4), DE/Fe_3O_4/TSAC dosage (0.024 g/100 mL), beginning chromium content (15 mg/L), and adsorption duration (60 min), the best removal of 93.28 % was achieved. The Langmuir, Freundlich, Temkin, Sips, and RedlichPeterson isotherm models were used to examine the adsorption data. With a maximum adsorption capacity for Cr (VI) of 131 mg/g, the results showed that the Freundlich and Langmuir isotherm models, along with Toth model, best matched the data. This implies that both monolayer and heterogeneous surface adsorptions are the main mechanism. The adsorption kinetics more closely match the pseudo-second-order model, revealing that the interactions betwixt Cr(VI) and the sorption sites is the rate-controlling stage of the process. The adsorption process is spontaneous, according to thermodynamic measurements, and it is endo-thermic, as evidenced by the negative ΔH° value. Furthermore, the recyclability of DE/Fe_3O_4/TSAC demonstrated excellent performance for five consecutive cycles, with adsorption efficiency of that is 93.26, 88.12, 84.15, 78.59, and 74.02 % for first, second, third, fourth and fifth runs, respectively. However, experiments were limited to controlled conditions, overlooking long-term stability and co-ion effects. Future research should, conduct pilot-scale studies, real wastewater testing, leaching control, and pilot-scale trials, and assess environmental impacts, to validate DE/Fe_3O_4/ TSAC practical application in Cr(VI) remediation.

CRediT authorship contribution statement

Sintayehu Shewatatek: Writing – original draft, Data curation, Investigation, Formal analysis, Validation. **Girma Gonfa:** Writing – review & editing, Supervision, Methodology, Writing – original draft. **Sintayehu Mekuria:** Investigation, Data curation, Writing – original draft. **Belete Tessema:** Investigation, Validation, Resources, Writing – original draft. **Gulmira Kezembayeva:** Data curation, Writing – original draft, Software. **Kalyan Sundar Ghosh:** Validation, Writing – review & editing, Writing – original draft, Software. **Muhammad Mushtaq:** Supervision, Writing – review & editing, Writing – original draft, Investigation. **Mohammad Hadi Diyanatizadeh:** Data curation. **Kaan Isinkaralar:** Writing – original draft. **Ahmad Hosseini-Bandegharaei:** Project administration, Writing – review & editing, Formal analysis, Supervision, Data curation, Methodology.

Declaration of competing interest

The authors declare that they have no known competing financial interests or personal relationships that could have appeared to influence the work reported in this paper.

Acknowledgments

Addis Ababa Science and Technology University is acknowledged for the financial support.

Appendix A. Supplementary data

Supplementary data to this article can be found online at https://doi.org/10.1016/j.rechem.2025.102486.

Data availability

Data will be made available on request.

References

[1] M. Asanu, D. Beyene, A. Befekadu, Removal of hexavalent chromium from aqueous solutions using natural zeolite coated with magnetic nanoparticles: optimization, kinetics, and equilibrium studies, Adsorpt. Sci. Technol. 2022 (2022) 8625489.
[2] B. Liu, et al., Removal of chromium species by adsorption: fundamental principles, newly developed adsorbents and future perspectives, Molecules 28 (2) (2023) 639.
[3] S. Duan, et al., Synthesis of magnetic biochar from iron sludge for the enhancement of Cr (VI) removal from solution, J. Taiwan Inst. Chem. Eng. 80 (2017) 835–841.
[4] A. Li, et al., High-efficiency removal of Cr (VI) from wastewater by mg-loaded biochars: adsorption process and removal mechanism, Materials 13 (4) (2020) 947.
[5] L. Rani, J. Kaushal, A. Lal Srivastav, Biochar as sustainable adsorbents for chromium ion removal from aqueous environment: a review, Biomass Convers. Biorefinery 14 (5) (2024) 6083–6096.
[6] Y. Liu, et al., Efficient removal of Cr (VI) from wastewater by magnetic biochar derived from peanut hull, Water Air Soil Pollut. 235 (2) (2024) 100.
[7] E. Nyankson, et al., Characterization and evaluation of zeolite a/Fe3O4 nanocomposite as a potential adsorbent for removal of organic molecules from wastewater, J. Chem. 2019 (1) (2019) 8090756.
[8] J. Fito, M. Abewaa, T. Nkambule, Magnetite-impregnated biochar of parthenium hysterophorus for adsorption of Cr (VI) from tannery industrial wastewater, Appl Water Sci 13 (3) (2023) 78.
[9] F. Kong, et al., Removal of Cr (VI) from wastewater by artificial zeolite spheres loaded with nano Fe–Al bimetallic oxide in constructed wetland, Chemosphere 257 (2020) 127224.
[10] A. Sanchez-Hachair, A. Hofmann, Hexavalent chromium quantification in solution: comparing direct UV–visible spectrometry with 1, 5-diphenylcarbazide colorimetry, C. R. Chim. 21 (9) (2018) 890–896.
[11] T.L. Tan, H. Nakajima, S.A. Rashid, Adsorptive, kinetics and regeneration studies of fluoride removal from water using zirconium-based metal organic frameworks, RSC Adv. 10 (32) (2020) 18740–18752.
[12] N. Belachew, H. Hinsene, Preparation of zeolite 4A for adsorptive removal of methylene blue: optimization, kinetics, isotherm, and mechanism study, Silicon 14 (4) (2022) 1629–1641.
[13] T.M. Zhang, et al., Preparation and characterization of AgA zeolite/polysulfone membranes, Adv. Mat. Res. 549 (2012) 401–405.
[14] W. Liu, et al., Efficient removal of hexavalent chromium from water by an adsorption–reduction mechanism with sandwiched nanocomposites, RSC Adv. 8 (27) (2018) 15087–15093.
[15] X. Jiang, et al., Removal of Cr (VI) from wastewater by a two-step method of oxalic acid reduction-modified fly ash adsorption, RSC Adv. 9 (58) (2019) 33949–33956.
[16] V.H. Nguyen, et al., Magnetic Fe3O4 nanoparticle biochar derived from pomelo peel for reactive red 21 adsorption from aqueous solution, J. Chem. 2020 (1) (2020) 3080612.
[17] M.H. Shemy, et al., Synthesis of green magnetite/carbonized coffee composite from natural pyrite for effective decontamination of Congo red dye: steric, synergetic, oxidation, and ecotoxicity studies, Catalysts 13 (2) (2023) 264.
[18] N. Inchaurrondo, et al., Natural diatomites: efficient green catalyst for Fenton-like oxidation of Orange II, Appl. Catal. Environ. 181 (2016) 481–494.
[19] T.A. Amibo, S.M. Beyan, T.M. Damite, Novel lanthanum doped magnetic teff straw biochar nanocomposite and optimization its efficacy of defluoridation of groundwater using RSM: a case study of hawassa city, Ethiopia, Adv. Mater. Sci. Eng. 2021 (2021) 1–15.
[20] S. Shewatatek, et al., Response surface optimization of Lead adsorption onto Teff straw-derived activated carbon, Results Surf. Interfaces 18 (2025) 100378.
[21] S.M. Beyan, et al., A statistical modeling and optimization for Cr (VI) adsorption from aqueous media via teff straw-based activated carbon: isotherm, kinetics, and thermodynamic studies, Adsorp. Sci. Technol. 2022 (2022) 7998069.
[22] K. Siraj, et al., The effect of microwave and muffle furnace-assisted heating on the surface characteristics of teff husk activated carbons: thermodynamic, isotherm, and kinetics study of Pb removal, Diamond Relat. Mater. 143 (2024) 110912.
[23] T.A. Amibo, S.M. Beyan, T.M. Damite, Novel lanthanum doped magnetic teff straw biochar nanocomposite and optimization its efficacy of defluoridation of groundwater using RSM: a case study of hawassa city, Ethiopia, Adv. Mater. Sci. Eng. 2021 (1) (2021) 9444577.

[24] K.-W. Jung, et al., Facile synthesis of magnetic biochar/Fe3O4 nanocomposites using electro-magnetization technique and its application on the removal of acid orange 7 from aqueous media, Bioresour. Technol. 220 (2016) 672–676.
[25] G. Lemessa, Y. Chebude, E. Alemayehu, Adsorptive removal of Cr (VI) from wastewater using magnetite–diatomite nanocomposite, AQUA—Water Infrastruct. Ecosyst. Soc. 72 (12) (2023) 2239–2261.
[26] S. Shewatatek, et al., Adsorptive removal of Cr (VI) from aqueous solution using sulfuric acid-treated diatomite, Results Chem. 15 (2025) 102205.
[27] T. Derbe, E.A. Zereffa, T. Sani, Synthesis of zeolite-a/Fe3O4/biochar composite for removal of Cr (VI) from aqueous solution, Int. J. Environ. Sci. Technol. 21 (16) (2024) 10027–10046.
[28] S. Shewatatek, et al., Response surface optimization of chromium (IV) removal with Teff straw-based activated carbon, Results Chem. 15 (2025) 102168.
[29] X. Shan, et al., Activated carbon/diatomite-based magnetic nanocomposites for magnetic solid-phase extraction of S-phenylmercapturic acid from human urine, Biomed. Chromatogr. 34 (7) (2020) e4834.
[30] T. Anirudhan, M. Ramachandran, Adsorptive removal of basic dyes from aqueous solutions by surfactant modified bentonite clay (organoclay): kinetic and competitive adsorption isotherm, Process Saf. Environ. Prot. 95 (2015) 215–225.
[31] A. Temesgen Abeto, et al., Optimization and modeling of Cr (VI) removal from tannery wastewater onto activated carbon prepared from coffee husk and sulfuric acid (H2SO4) as activating agent by using central composite design (CCD), J. Environ. Public Health 2023 (1) (2023) 5663261.
[32] K. Sardar, et al., Heavy metals contamination and what are the impacts on living organisms, Greener J. Environ. Manage. Public Safety 2 (4) (2013) 172–179.
[33] Kusuma, H.S., et al. Response surface methodology (RSM) modeling of microwave-assisted extraction of natural dye from Swietenia mahagony: a comparation between box-Behnken and central composite design method. In AIP conference proceedings. 2015. AIP Publishing.
[34] Kusuma, H.S. and M. Mahfud. Box-Behnken design for investigation of microwave-assisted extraction of patchouli oil. In AIP Conference Proceedings. 2015. AIP Publishing.
[35] B. Tessema, et al., Synthesis and characterization of silver nanoparticles using reducing agents of bitter leaf (Vernonia amygdalina) extract and tri-sodium citrate, Nano-Structures & Nano-Objects 35 (2023) 100983.
[36] S. Shewatatek, et al., Response surface optimization of lead adsorption onto teff straw-derived activated carbon, Results in Surfaces and Interfaces 18 (2025) 100378.
[37] Jiang, H.-m., et al., Zincon-immobilized silica-coated magnetic Fe3O4 nanoparticles for solid-phase extraction and determination of trace lead in natural and drinking waters by graphite furnace atomic absorption spectrometry. Talanta, 2012. 94: p. 251–256.
[38] Z. Zhang, J. Kong, Novel magnetic Fe3O4@ C nanoparticles as adsorbents for removal of organic dyes from aqueous solution, J. Hazard. Mater. 193 (2011) 325–329.
[39] Y.-P. Chang, et al., Preparation and characterization of hexadecyl functionalized magnetic silica nanoparticles and its application in rhodamine 6G removal, Appl. Surf. Sci. 257 (20) (2011) 8610–8616.
[40] D. Mohan, et al., Development of magnetic activated carbon from almond shells for trinitrophenol removal from water, Chem. Eng. J. 172 (2–3) (2011) 1111–1125.
[41] J. Wang, et al., Amino-functionalized Fe3O4@ SiO2 core–shell magnetic nanomaterial as a novel adsorbent for aqueous heavy metals removal, J. Colloid Interface Sci. 349 (1) (2010) 293–299.
[42] A. Donia, A. Atia, F. Abouzayed, Preparation and characterization of nano-magnetic cellulose with fast kinetic properties towards the adsorption of some metal ions, Chem. Eng. J. 191 (2012) 22–30.
[43] V. Ranjithkumar, et al., Magnetic activated carbon-Fe3O4 nanocomposites—synthesis and applications in the removal of acid yellow dye 17 from water, J. Nanosci. Nanotechnol. 14 (7) (2014) 4949–4959.
[44] Z. Akbari-Jonoush, et al., Application of C14/SiO2–Fe3O4 and AC–Fe3O4 nanocomposite for U (VI) removal, Desalin. Water Treat. 57 (47) (2016) 22519–22532.
[45] M. Kosmulski, The pH dependent surface charging and points of zero charge. IX. Update, Adv. Colloid Interface Sci. 296 (2021) 102519.
[46] T. Kokab, et al., Effective removal of Cr (vi) from wastewater using biochar derived from walnut shell, Int. J. Environ. Res. Public Health 18 (18) (2021) 9670.
[47] H. Qi, et al., Adsorption of chromium (VI) by cu (I)-MOF in water: optimization, kinetics, and thermodynamics, J. Chem. 2021 (1) (2021) 4413095.
[48] C. Santhosh, et al., Synthesis and characterization of magnetic biochar adsorbents for the removal of Cr (VI) and acid orange 7 dye from aqueous solution, Environ. Sci. Pollut. Res. 27 (2020) 32874–32887.
[49] B. Szala, T. Bajda, A. Jeleń, Removal of chromium (VI) from aqueous solutions using zeolites modified with HDTMA and ODTMA surfactants, Clay Miner. 50 (1) (2015) 103–115.
[50] Brungesh, K., et al., An efficient removal of toxic Cr (VI) from aqueous solution by MnO2 coated polyaniline nanofibers: kinetic and thermodynamic study. J. Environ. Anal. Toxicol., 2017. 7(2161): p. 2161–0525.1000442.
[51] P. Qiu, et al., Application of box-Behnken design with response surface methodology for modeling and optimizing ultrasonic oxidation of arsenite with H2O2, Open Chem. 12 (2) (2014) 164–172.
[52] N.K. Mondal, et al., Optimization of Cr (VI) biosorption onto aspergillus Niger using 3-level box-Behnken design: equilibrium, kinetic, thermodynamic and regeneration studies, J. Genet. Eng. Biotechnol. 15 (1) (2017) 151–160.
[53] L. Giraldo, A. Erto, J.C. Moreno-Piraján, Magnetite nanoparticles for removal of heavy metals from aqueous solutions: synthesis and characterization, Adsorption 19 (2013) 465–474.
[54] M. Shahadat, S. Isamil, Regeneration performance of clay-based adsorbents for the removal of industrial dyes: a review, RSC Adv. 8 (43) (2018) 24571–24587.
[55] M. Fayazi, M. Ghanbarian, One-pot hydrothermal synthesis of polyethylenimine functionalized magnetic clay for efficient removal of noxious Cr (VI) from aqueous solutions, Silicon 12 (1) (2020) 125–134.
[56] P. Belibağlı, B.N. Çiftci, Y.U. Uysal, Chromium (Cr (VI)) removal from water with bentonite-magnetite nanocomposite using response surface methodology (RSM), Sigma Journal of Engineering and Natural Sciences 38 (3) (2020) 1217–1233.
[57] Z. Sun, et al., In situ synthesis of carbon@ diatomite nanocomposite adsorbent and its enhanced adsorption capability, Part. Sci. Technol. 35 (4) (2017) 379–386.
[58] T. Altun, Preparation and application of glutaraldehyde cross-linked chitosan coated bentonite clay capsules: chromium (VI) removal from aqueous solution, J. Chil. Chem. Soc. 65 (2) (2020) 4790–4797.
[59] F.A. Bezza, E.M. Chirwa, Removal of chromium (vi) ions from polluted water using kaolinite supported Fe/Al oxide (hydroxide) composite Nanoadsorbents, Chem. Eng. Trans. 94 (2022) 1453–1458.
[60] Z. Deng, et al., Removal of phosphate from aqueous solution by zeolite-biochar composite: adsorption performance and regulation mechanism, Appl. Sci. 12 (11) (2022) 5334.
[61] R. Khamirchi, et al., Adsorption property of Br-PADAP-impregnated multiwall carbon nanotubes towards uranium and its performance in the selective separation and determination of uranium in different environmental samples, Ecotoxicol. Environ. Saf. 150 (2018) 136–143.